University of Crete
Department of Physics

Undergraduate Thesis

# Generation of intense ultrashort pulses in the UV region

*Author:*
Ioannis Thyris

*Supervisors:*
Prof. D. Charalambidis
Dr. P. Tzallas

Heraklion
June, 2015

# Contents

# Acknowledgements

The present thesis is a part of my undergraduate studies. I would like to use this opportunity to thank all the people that have supported me throughout my undergraduate years and the people that helped to complete this thesis.

Firstly, I would like to thank Prof. Dimitris Charalambidis for introducing me to the field of ulrashort pulses and for giving me the opportunity to do my undergraduate thesis in this exciting field. Secondly, I would like to thank Dr. Paraskevas Tzallas for his instructions and for recommending the topic of this thesis.

Then, I would like to thank all the members of the research group for making me feel comfortable while being around. I specifically would like to thank Manolis Skantzakis for his useful tips and Dr. David Gray for showing the basics in the lab, as well as for giving me an overview of the laser system.

Of course, I cannot but express my gratitude to Giorgos Kolliopoulos. I would like to thank him for his guidance throughout this past year. The many fruitful discussions we had were invaluable to me. His patience with me and his encouragement truly inspired me in times when all seemed grim. It is certain that the present thesis would be much different without his contribution, if possible at all.

Next, I would like to thank my family for always having faith in me and for always supporting me. I would like to thank them for giving me the possibility to study something that I enjoy and for their financial and emotional support throughout my studies. Additionally, I would like to thank all of my friends for always brightening my mood, even during the hardest of times. Thank you for all the laughs and for all the thought-provoking discussions. Lastly, I would like to thank my partner Ioanna, for her patience, for showing understanding and for her encouragement in difficult times.

*In the memory of my uncles, Vassilis and Manolis*

# Introduction

For the last century and a half we have been studying phenomena that occur on shorter and shorter time scales. In order to record and study fast phenomena we need a mechanism that can provide a temporal variation comparable to the characteristic time of the phenomena. At first, mechanical shutters were used to record moving horses, with $ms$ resolution and later flashes of light were used to record bullets splitting apples with $\mu s$ resolution. However, if we want to record phenomena that occur down to the atomic scales, we need the means to provide such temporal resolution. For reference, the atomic unit for time is: $t_{a.u.} = 24as = 24 \times 10^{-18} sec$.

With the invention of the laser, have been able to manipulate many nonlinear processes to our advantage and as a result we have been able to produce pulses with duration of few femtoseconds, or even sub-femtosecond pulses. Thus, the means to record phenomena that occur on the atomic scale have been made possible.

Here, we investigate the generation of intense ultrashort pulses in the UV region. We are particularly interested in the UV region, which ranges from $100nm$ to $400nm$, because many molecules have absorption lines in this region. By having short pulses in the UV region, we can study electron and nuclear dynamics in molecules through time resolved spectroscopy. This can be done using an initial pulse (pump) which coherently excites the molecule. Then, after a variable time delay a second pulse (probe) interacts with the molecule and by the product yield of the interaction as a function of the delay between the pump and the probe pulses, we can study the electron or nuclear wavepacket time-evolution.

One way to achieve pulses with wavelengths in the UV region is through harmonic generation. Assuming a driver field of central wavelength at $800nm$, its third ($270nm$) and fifth ($160nm$) harmonic will be in the wavelength range of interest. In this thesis we do a numerical simulation of the third-harmonic generation process when using the polarization gating apparatus. The results of this calculation will be used as an input to the development of an experimental setup in IESL-FORTH. The numerical results were obtained

using a code written in Wolfram Mathematica for the needs of this thesis. Similar calculation can be done for the firth-harmonic as well.

In the first chapter some theoretical background will be presented for low-harmonics, as well as for high-harmonics in order to note the different generation processes. Using this background we will investigate the third-harmonic generation. In the second chapter, the polarization gating technique, a core component in our calculation, will be discussed. In the third chapter the numerical results will be presented, while in the last chapter an experimental arrangement will be proposed.

# Chapter 1

# Theory

The nonlinear response of matter to intense radiation manifests itself in a nonlinear dependence of the induced polarization on the electric field of the incident radiation [4]. The nonlinearity can originate from different processes. For example, for intensities which are low to moderate ($< 10^{13} W/cm^2$), the external laser field is much weaker than the static atomic Coulomb field. Nonlinear interactions taking place under these conditions can be well described by a perturbative approach, and we refer to this parameter range as the *regime of perturbative nonlinear optics* (Figure 1b). When the electric field strength becomes comparable or higher than the binding Coulomb field experienced by the outer-shell electrons, an electron can escape from its bound state via tunneling before the laser electric field reverses its sign. This parameter range giving rise to these processes is called as *strong-field regime* of nonlinear optics.

Of the nonlinear processes, arguably the most important, widely studied and used is the harmonic generation, originating back to 1961 when for the first time the second harmonic was generated[16]. Generally speaking, the process in which an incident wave of frequency $\omega$ is upconverted in a medium, such as crystals and gases, producing a wave of frequency $q\omega$, with $q$ being the harmonic order is called harmonic generation.

The production of low order harmonics is a pertubative nonlinear process that occurs when a laser field is driven into a medium with sufficient intensity. In a classical approach, the incident wave, called driver, induces polarization on the medium, which has a nonlinear dependence on the driver electric field. As a result, the medium in return radiates at different frequencies, which are integer multiples of the frequency of the driving field. This can be better understood in the quantum approach (Figure 1.1a), in which the harmonic generation is a multiphoton process. An atom of the medium with ionization energy $E_I$ absorbs $q$ photons with energy $\hbar\omega$ and is excited to

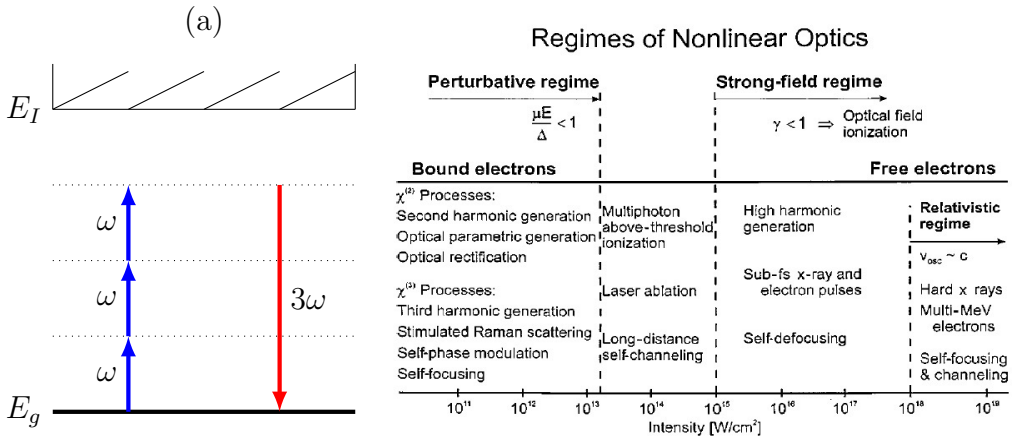


Figure 1.1: (a) The process of the third-harmonic generation from an energy level standpoint. The thick solid line is the ground stare with energy $E_g$, the dotted lines indicate virtual states and the angled lines indicate states in the continuum. (b) The different regimes of nonlinear optics [4]. The boundaries between different regimes are not sharply defined, but depend on the atom in question.

a virtual state. The atom then emits a photon with energy $q\hbar\omega$, which is the harmonic radiation and it is a low harmonic when $q\hbar\omega < E_I$. This is described by perturbation theory and will be analyzed in the next chapter.

On the other hand, for the high harmonic generation, a process in the strong-field regime, a semi-classical model, called the *three-step model* was proposed in 1993 [24, 11]. It involves tunneling ionization of the atom, acceleration of the free electron due to the electric field and the recombination of the electron with the parent core.

It is important to note the difference of the mechanism of the production of high and low harmonics. In contrast to the high harmonic generation (HHG), the low harmonic generation does not involve ionization of the atom but, is in a sense, a multiphoton scattering process. As a result, the low and high harmonics have different dependence on various important quantities, such as the ellipticity, the dependence of the intensity on the harmonic order etc. The high harmonic process will be discussed briefly in the last section of this chapter, in order to shed light to this fundamental issue. For the remainder of this thesis, we will be focused on the perturbative regime, unless stated otherwise.

## 1.1 Low harmonic generation

When a wave with electric field $\vec{\mathscr{E}}$ is propagating through a conducting medium with polarization $\vec{\mathscr{P}}$, the wave equation describing it is:

$$\nabla^2\vec{\mathscr{E}} - \frac{1}{c^2}\frac{\partial^2\vec{\mathscr{E}}}{\partial t^2} = \frac{4\pi}{c^2}\frac{\partial^2\vec{\mathscr{P}}}{\partial t^2} \ . \tag{1.1}$$

In order to describe the nonlinear optical interaction, one must know the dependence of the polarization on the optical fields. In the most general form the polarization is a functional of the optical fields [32, 3]:

$$\mathscr{P}(r,z,t) = f\big(\mathscr{E}(r,z,t), \mathscr{E}(r'',z'',t'')\big) \ . \tag{1.2}$$

The exact expression of the polarization is dependent on the atomic properties of the medium and is a rather difficult task to retrieve. Thus, several assumptions and approximations are made in order to simplify the form of the polarization.

Firstly,we expand the polarization in terms of the moments of the charge distribution, i.e. we make an expansion of the polarization in which each term is attributed to the different terms of the multipole expansion. In this approximation we have:

$$\mathscr{P}(r,z,t) = P(r,z,t) + \mathbb{P}(r,z,t) + \cdots \ , \tag{1.3}$$

the first term corresponds to the dipole polarization, the next to the quadrupole polarization and so on.

In the general case the time-dependent polarizations that are needed for Eq. 1.1 can be quite complicated, so it is useful to consider the Fourier components of the polarization. At this point we assume that the electric fields we are dealing with are sufficiently weak compared to the atomic fields that bind the electrons in the medium. Under these conditions, one can expand the Fourier components of each term in Eq. 1.3 in the Fourier components of the powers of the optical fields as:

$$\begin{aligned}\mathscr{P}_T(r,z,\omega) =& \chi^{(1)}(\omega)\mathscr{E}_T(r,z,\omega) + \{\chi^{(2)}(\omega)\mathscr{E}_T^2(r,z)\}_\omega + \{\chi^{(3)}(\omega)\mathscr{E}_T^3(r,z)\}_\omega + \cdots \\ & Q^{(1)}(\omega)\nabla\mathscr{E}_T(r,z,\omega) + Q^{(2)}(\omega)\{\nabla_T\mathscr{E}_T^2(r,z)\}_\omega + \\ & Q^{(3)}(\omega)\{\nabla_T\mathscr{E}_T^3(r,z)\}_\omega + \cdots \ .\end{aligned} \tag{1.4}$$

In the above equation, the coefficients of the various terms are know as the $n$th-order $m$-pole susceptibilities. The symbol $\mathscr{E}_T(\omega)$ is the Fourier transform of the electric field and the symbol $\{\ \}_\omega$ indicates that only the Fourier component at frequency $\omega$ of the quantity in braces must be considered.

Using Eq. 1.4 we can write the polarization as a sum of the linear and nonlinear terms:

$$\mathscr{P}_T(\omega) = \mathscr{P}_T^L(\omega) + \mathscr{P}_T^{NL}(\omega) \ , \tag{1.5}$$

with

$$\mathscr{P}_T^L(\omega) = \chi^{(1)}(\omega)\mathscr{E}_T(\omega) + Q^{(1)}(\omega)\nabla\mathscr{E}_T(\omega) + \cdots \tag{1.6}$$

and

$$\begin{aligned}\mathscr{P}_T^{NL}(\omega) =& \{\chi^{(2)}\mathscr{E}_T^2\}_\omega + \{\chi^{(3)}\mathscr{E}_T^3\}_\omega + \cdots \\ &+ Q^{(2)}\{\nabla_T\mathscr{E}_T^2\}_\omega + \ Q^{(3)}\{\nabla_T\mathscr{E}_T^3\}_\omega + \cdots \ .\end{aligned} \tag{1.7}$$

So far we have used all the terms in polarization from the multipole expansion. However, because the dipole terms are usually much stronger than the corresponding higher multipole terms, the expansion in Eq. 1.3 converges rapidly in the wavelength in the range of interest of this thesis (IR), with the dipole polarization being dominant. That is not the case when the wavelength is comparable with the characteristic dimensions of the medium. The higher order terms become more significant as the wavelength of the driving fields drops to the X-ray region, where the wavelength is of the same order as the size of an atom [44]. For this study, in which the driving laser pulse had its peak intensity at 800nm, using only the dipole terms is considered a good approximation.

It's more convenient to obtain a perturbation expansion for the polarization in the time domain by taking the inverse Fourier transform of each term in Eq. 1.4. Using the justification above, we can use only the dipole terms. Taking the inverse Fourier transform we have:

$$\mathcal{F}^{-1}\{\mathscr{P}_T\} = \mathcal{F}^{-1}\{\chi^{(1)}\mathscr{E}_T\} + \mathcal{F}^{-1}\{\chi^{(2)}\mathscr{E}_T^2\} + \mathcal{F}^{-1}\{\chi^{(3)}\mathscr{E}_T^3\} + \cdots \ , \tag{1.8}$$

where $\mathcal{F}^{-1}$ is the inverse Fourier transform operator.

Using the convolution theorem which states that: $\mathcal{F}^{-1}\big\{\mathcal{F}\{f\}\mathcal{F}\{g\}\big\} = f * g$, where the $*$ symbol indicates the convolution of the two functions $f$ and $g$, we get that the polarization in the time domain is the sum of convolutions between the powers of the time-dependent fields with the time-dependent response functions of the medium. When the characteristic response time of the polarization components of the medium is significantly faster than the time scale in which the field amplitudes vary, the convolution integrals can be

replaced with simple products. Then the time-dependent dipole polarization is:

$$\mathscr{P}_T(t) = \boldsymbol{\chi}^{(1)}\mathscr{E}_T(t) + \boldsymbol{\chi}^{(2)}\mathscr{E}_T^2(t) + \boldsymbol{\chi}^{(3)}\mathscr{E}_T^3(t) + \boldsymbol{\chi}^{(4)}\mathscr{E}_T^4(t) + \cdots \ . \tag{1.9}$$

The coefficients of the powers of the fields in Eq. 1.9 are in bold to indicate that they represent the time-dependent response of the medium rather than the response in the frequency domain, as in Eq. 1.4. They are constants that are determined by the properties of the medium and are derived in many nonlinear optics textbooks [3].

We now have the perturbative expansion of the polarization which can be used to solve Eq. 1.1, which is done in many non-linear optics textbooks, and extract important properties of the harmonics. In the next chapter we will present some important properties of low-harmonics obtained by solving Eq. 1.1, or straight from Eq. 1.9.

## 1.2 Properties of low harmonics

### Harmonics of even order

Firstly, lets assume that the medium in question has inversion symmetry [32]. We then write the second-order polarization:

$$\mathscr{P}_T^{(2)} = \boldsymbol{\chi}^{(2)}\mathscr{E}_T^2 \ . \tag{1.10}$$

If we invert the coordinate system ($r \to -r = r'$) and write the inverted variables with primes, we have:

$$\mathscr{P}_T'^{(2)} = \boldsymbol{\chi}'^{(2)}\mathscr{E}_T'^2 \ . \tag{1.11}$$

When the coordinate system is inverted both the polarization and the electric field must change sign while the susceptibility, which carries the symmetry of the medium, cannot:

$$\mathscr{P}_T = -\mathscr{P}_T', \ \mathscr{E}_T = -\mathscr{E}_T', \ \boldsymbol{\chi}^{(2)} = \boldsymbol{\chi}'^{(2)} \ .$$

Using these relations, Eq.1.11 becomes:

$$\mathscr{P}_T^{(2)} = -\boldsymbol{\chi}^{(2)}\mathscr{E}_T^2 \tag{1.12}$$

The only way for Equations (1.10) and (1.12) to be compatible for each other is if $\boldsymbol{\chi}^{(2)} = 0$. Similar reasoning can be applied to show that all even-order dipole susceptibilities are zero in media with inversion symmetry. This is an

important result which is general and even stands for the high harmonics as well: centrosymmetric media cannot generate even-order harmonics in the dipole approximation. Typical non centrosymmetric media are some crystals and surfaces, in contrast with gases which are centrosymmetric.

## Frequency

While the electric field $\mathscr{E}$ is a real quantity, mathematically it is more convenient to use the complex representation. Therefore, we can express an optical laser pulse by its time-dependent electric field as [6]:

$$\epsilon(t) = E(t)e^{i\omega_0 t} \ , \tag{1.13}$$

with $E(t)$ being the time-dependent amplitude (envelope), $\omega_0$ the carrier (central) angular frequency and $\epsilon(t)$ follows the relation $\mathscr{E}(t) = Re\{\epsilon(t)\}$. Using Eq.1.9 and the expression of the electric field of the pulse we see that each term in the perturbative expansion oscillates with angular frequency which is an integer multiple of the central frequency $\omega_0$. For example, it is clear that the third harmonic which has the frequency $3\omega_0$ originates from the term $\chi^{(3)}\mathscr{E}_T^3$.

Note that while the linear term in Eq. 1.9 describes polarizations at frequency $\omega$ which arise from fields with the same frequency, the nonlinear terms connect polarizations at a frequency $\omega$ to a number of fields that can be at different frequencies. To be more specific, for example a polarization of frequency $\omega = \omega_1 + \omega_2$ can be generated by two fields $\mathscr{E}_1$ and $\mathscr{E}_2$ with frequencies $\omega_1$ and $\omega_2$ respectively, through a second order term.

## Intensity

The $q$-th harmonic intensity $I_{q\omega}$ varies as the $q$th power of the fundamental intensity [31]:

$$I_{q\omega}(t) \propto I_{\omega}^{q}(t) \ . \tag{1.14}$$

This power law dependence is to be expected for a perturbative $q$-photon process, since $R_q = \sigma_q I^q$, where $R_q$ is the rate of the $n$-photon process, $\sigma_q$ is the atomic cross section of the process and $I_q$ is the laser intensity. The power spectrum of the harmonics generated in the perturbative regime is described by Eq.1.14.

## Time duration

Let's assume a Gaussian envelope of the driving pulse, the normalized intensity is then: $I(t) = e^{\left(-4\ln 2(\frac{t}{\tau_\omega})^2\right)}$ , where $\tau_\omega$ is the FWHM of the pulse. Using

Eq.1.14 we have [6]:

$$I_{q\omega}(t) \propto I_{\omega}^{q}(t) \Leftrightarrow e^{\left(-4\ln 2\frac{t^2}{\tau_{q\omega}^2}\right)} = \left[e^{\left(-4\ln 2\frac{t^2}{\tau_{\omega}^2}\right)}\right]^q = e^{\left(-4q\ln 2\frac{t^2}{\tau_{\omega}^2}\right)} \tag{1.15}$$

Comparing the left and the right hand side of the above equation we come to the important result for the time duration of the harmonic:

$$\tau_{q\omega} = \frac{\tau_{\omega}}{\sqrt{q}} \ . \tag{1.16}$$

This is the case for the high harmonics as well. For a driver pulse with FWHM of $20fs$ Eq. 1.16 suggests that FWHM of its third harmonic is $\simeq 11,5fs$ and of its fifth to be $\simeq 8.9fs$. Using harmonics of higher orders in the perturbative regime, we could potentially achieve shorter pulses, but the intensity decreases exponentially with the harmonic order.

## Ellipticity

A general solution for a plane wave propagating in the direction $\mathbf{k}$ is given by [22]:

$$\mathbf{E}(\mathbf{x},t) = (\boldsymbol{\epsilon}_1 E_1 + \boldsymbol{\epsilon}_2 E_2) e^{i\mathbf{k}\cdot\mathbf{x} - i\omega t} \ , \tag{1.17}$$

where the amplitudes $E_1$ and $E_2$ are complex numbers, allowing the possibility of phase difference between the waves of the two transverse directions $\boldsymbol{\epsilon}_1$ and $\boldsymbol{\epsilon}_2$.

When $E_1$ and $E_2$ do not have the same magnitude and their phases obey the relation: $n\pi < \phi_1 - \phi_2 < (n + \frac{1}{2})\pi$ , the wave is called to be elliptically polarized. In other words, the end point of the electric field is inscribed in an ellipse (Figure 1.2a).

In general, the axes of the ellipse are not in the $0x$ and $0y$ directions, but the ellipse is inclined at an angle $\alpha$ with respect to the $x$-axis which is given by the expression [15]:

$$\tan(2\alpha) = \frac{2E_{0x}E_{0y}\cos\theta}{E_{0x}^2 - E_{0y}^2} \ , \tag{1.18}$$

where $\theta = \phi_y - \phi_x$ is the phase difference of the two components $E_{0x}$ and $E_{0y}$ that are along the $x$ and $y$ axis respectively.
The ellipticity $\epsilon$ of the field is given by [40] :

$$\epsilon(t) = \tan\left[\frac{1}{2}\sin^{-1}\left(\frac{2|\vec{E}_1(t)|\ |\vec{E}_2(t)|\sin(\phi_x - \phi_y)}{|\vec{E}_1(t)|^2 + |\vec{E}_2(t)|^2}\right)\right] \ . \tag{1.19}$$

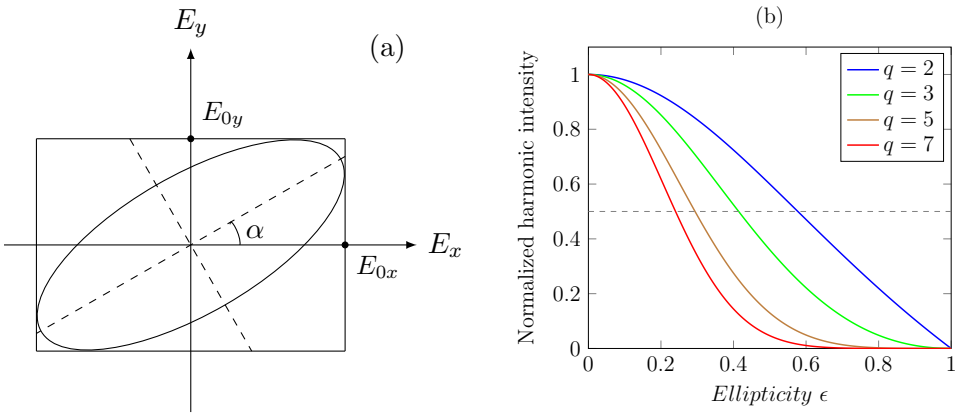


Figure 1.2: (a) Elliptically polarized light oriented at an angle relative to the x-axis. (b) Normalized harmonic Intensity as a function of the ellipticity of the driving pulse for different low-order harmonics.

As seen by the above equation, when $\epsilon = 0$ the field is linearly polarized and when $\epsilon = 1$ the field is circularly polarized.

Due to selection rules, the conversion efficiency of the harmonic generation process is dependent on the ellipticity of the driving field. The selection rules favor linear polarization and suggest that circular polarization does not produce harmonics. This can be seen by the symmetry relations of the susceptibility components [32]. The dependence of the low-harmonic intensity on the ellipticity $\epsilon$ and order $q$ (Figure 1.2b) is [5] :

$$I_q = \left(\frac{1-\epsilon^2}{1+\epsilon^2}\right)^{(q-1)} . \tag{1.20}$$

There is a value of ellipticity called ellipticity threshold $\epsilon_{th}$ for which the harmonic intensity becomes half the maximum ($I_q = I_q^{max}/2$). For example, for the third harmonic $\epsilon_{th}^{(3)} = 0.414$ and for the fifth $\epsilon_{th}^{(5)} = 0.294$.

One can use the dependence of the conversion efficiency on the ellipticity of the driving field to produce shorter harmonic pulses [12]. This is called polarization gating technique and it was first used for high-harmonic generation. Briefly, the driving pulse is modulated to have circular polarization at its edges and linear at its center. In other words, the pulse has time-dependent ellipticity, which reaches zero only near the center of the pulse. As a result, the harmonic generation is limited only near the center of the driving pulse, which is the most energetic part. Polarization gating will be discussed in the next chapter in more detail.

## 1.3 Conversion Efficiency

As mentioned before, when a laser pulse (driver) is focused on a gas jet, harmonics of the driving pulse are produced. However, one important aspect of the harmonic generation is the *conversion efficiency*, a measure of the effectiveness with which the power of the driver pulse is transferred to the harmonics [33] . In other words, the conversion efficiency is what determines the energy content of the harmonic pulse. In this section, we will qualitatively discuss some of the competing effects limiting the conversion efficiency. A proper treatment of this subject requires consideration of all possible competing effects simultaneously, which is a complex task requiring numerical evaluation for systems with known parameters such as the focus of the beam, the length of the interaction, the pulse duration, the atomic or molecular structure properties of the target etc. In practice, the conversion efficiency is given experimentally because of its dependence to the experimental parameters.

The first process that will be discussed here is multiphoton absorption. Generally, multiphoton absorption that is induced by the driving intensity can be expected to be the most important since the waves of the fundamental are usually the strongest. However, in experiments in which there is significant conversion of the generated wave, nonlinear absorption induced by the generated intensity can also be important. Secondly, the medium can be ionized through multiphoton ionization of two or more photons from the pump or generated waves or from both simultaneously. When the intensity of the driver gets sufficiently high, the medium is characterized by a very high electron density. Another process which affects the conversion efficiency is the Stark shift of the energy levels of the medium. These processes affect the conversion efficiency in four ways [33]. They can result in energy loses at the driver or the harmonic pulse, they can cause saturation of the nonlinear susceptibility and can cause intensity-dependent phase changes that result in phase mismatching along with self-focusing and self-defocusing. The loss of *phase matching* (phase mismatching) plays a crucial role on the energy content of the harmonic pulse, so we find it important to discuss it in more detail in the next paragraph. This is the case in high-harmonics as well.

### 1.3.1 Phase mismatching

A laser pulse can be described in the time domain such as in Eq. 1.13. It can also be described in the frequency domain, where the electric field is obtained

by performing a Fourier transform of the field in the time domain [6] :

$$\tilde{E}(\omega) = \int_{-\infty}^{+\infty} \epsilon(t) e^{i\omega_0 t} dt \ . \tag{1.21}$$

In general, the transform gives:

$$\tilde{E}(\omega) = U(\omega) e^{i\phi(\omega)} \ , \tag{1.22}$$

with $U(\omega)$ being the spectral amplitude and $\phi(\omega)$ being the spectral phase.

A pulse propagating in an absorptive and dispersive material, the electric field exiting the medium can be described in the frequency domain as:

$$\tilde{E}_{out}(\omega) = \tilde{E}_{in}(\omega) e^{i\frac{\omega}{c}\tilde{n}(\omega)L} \ , \tag{1.23}$$

where $L$ is the length of the medium and $\tilde{n}(\omega)$ is the complex index of refraction of the material.

The phase of the low-harmonic wave is inherited by the pump wave [2]. Because the medium that the harmonic pulse is generated in is generally dispersive (i.e. the refractive index depends on the frequency), the driver pulse and the harmonic pulse propagate with different group velocities. In addition, the harmonic generation is not a single atom response of the medium, but a collective effect. As a result, the harmonic waves that are generated from different atoms along the medium gain different phases depending on where they are generated [4].

Imagine an atom at position $z_0$ through which the nonlinear process takes place and generates a harmonic wave (Figure 1.3a). The harmonic wave generated and the fundamental wave are co-propagating in the $z$ direction. Next, imagine an atom at position $z_1$ from which a harmonic wave will be generated as well. Due to the chromatic dispersion of the medium, the group velocities for the fundamental and the harmonics are different, thus the harmonic wave generated from $z_0$ and the one generated from $z_1$ will have different phases. As a result, contributions from different locations to the generated wave are not in phase at the end of the medium [14] . The destructive interference of harmonic waves generated at different locations in the medium can be viewed as the decrease on the conversion efficiency. This is called phase mismatching and it plays a crucial role in the reduction of the conversion efficiency. The experimental parameters need to be optimized in order to achieve phase-matching conditions.

Assuming weak pump field or non depleted media, the dependence of the harmonic intensity $I_q$ to the phase mismatching $\Delta k$ is [31] (Figure 2b):

$$I_q \propto \frac{\sin^2(\Delta k L/2)}{(\Delta k L/2)^2} \ . \tag{1.24}$$

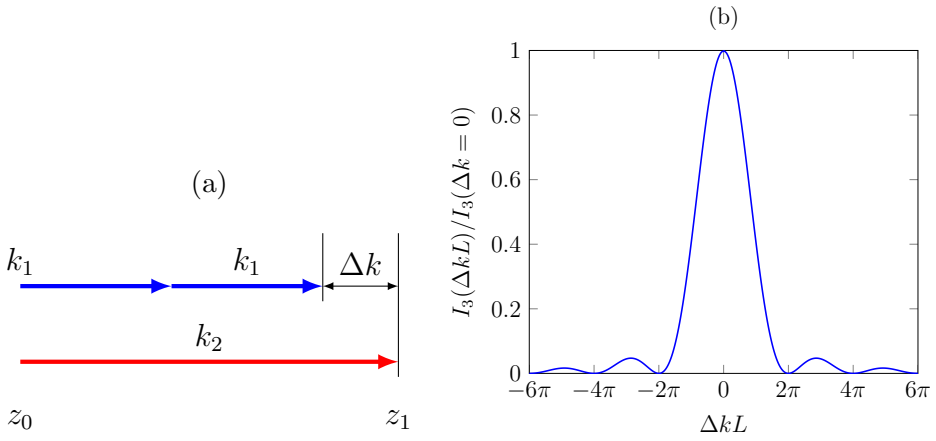


Figure 1.3: (a) Phase mismatch for second-harmonic generation. Due to chromatic dispersion the wavenumber of the harmonic is more than twice as large as that for the fundamental wave. (b) Plot of the normalized third-harmonic intensity as a function of the phase mismatch.

From Eq. 1.24 we see that the harmonic intensity oscillates as a function of the interaction length. Maxima in the harmonic intensity occur at odd multiples of the coherence length $L_c$ [30], which is given by:

$$L_c = \pi/\Delta k \tag{1.25}$$

At this distance the harmonic field has slipped in phase by $\pi$ rad relative to its driving field. It is essentially a measure of the dimensions of the medium to be used, because increasing the length of the medium beyond the coherence length does not translate in an increase to the harmonic amplitude but rather to a decrease [14, 4] .

Another important effect that plays a crucial role in phase matching is the production of plasma in the medium. As the driver pulse propagates through the medium, it ionizes the medium producing free electrons. Although the free electrons make a negative contribution to the refractive index, they make a positive contribution to the wave vector mismatch [9]. As a result, increasing the intensity of the driver pulse may not translate to an increase to the harmonic intensity, due to the increase to the free electron density. Above a critical density, the medium is saturated and the harmonic yield is decreasing. In addition, with increasing the driver pulse duration the ionization rate increases as well. This is because, more atoms of the medium get ionized from the driver pulse before the driver pulse can acquire its maximum intensity. When the duration is short, on the other hand, the atoms of the medium are exposed to high intensities for shorter times, thus reducing the

ionization rates, which results in higher conversion efficiencies [45, 38].

## 1.4 High Order Harmonic Generation

As mentioned before, the high harmonic generation (HHG) is a nonlinear process in the strong field regime, involving ionization of the atom. Different regimes of ionization of an atom can be distinguished using the *Keldysh paramater* which is given by [23]:

$$\gamma = \sqrt{\frac{I_p}{2U_p}} \ , \tag{1.26}$$

where $I_p$ is the ionization potential and $U_p$ is the cycle averaged kinetic energy of the electron gained from the electric field. This is also called ponderomotive energy and is given by:

$$U_p = \frac{e^2 E^2}{4m\omega^2} \tag{1.27}$$

where $E$ and $\omega$ are the electric field and the angular frequency of the light respectively, $e$ and $m$ are the charge and the mass of the electron. To give perspective, the Coulomb electric field in a hydrogen atom is $\approx 5 \times 10^9 V/cm$ corresponding to an equivalent intensity of $I_p \approx 3 \times 10^{16} W/cm^2$.

When $\gamma > 1$ the laser period is shorter than the tunneling time and thus the multiphoton ionization dominates, in which the atom absorbs a certain number of photons in order to be ionized. This is described by the lowest order perturbation theory [30, 4].

When $\gamma < 1$, the main ionization process is the tunneling of the electron through the strong suppression of the atomic potential by the electric field.

In the 'grey' area of $\gamma \approx 1$, their combination co-exists. The electrons are 'heated' up while moving under the barrier, leading to multiphoton absortion from under the potential barrier, best called 'non-adiabatic tunneling [21].

The *three step model* (Figure 1.4) is a classical model that was proposed in 1993 [11, 24], revealing the mechanism of high-order harmonic generation. Consider the interaction of a hydrogen atom with a linearly polarized field. As the intensity reaches about $10^{14} W/cm^2$, the field near the peak of each oscillation is comparable to the atomic Coulomb field. The superposition of the laser field and the Coulomb field transforms the potential well that binds the electron into a potential barrier. As a result, the electron tunnels in the continuum through the barrier suppressed by the field (first step). The freed electron is then accelerated by the electric field. In one laser cycle,

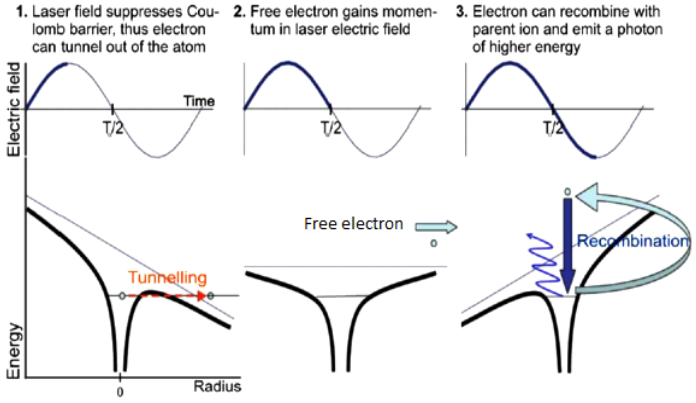


Figure 1.4: The three step model [11]. At the top is the electric field in each of the steps and at the bottom is the atomic response to the field [27].

the electron first moves away from the nucleus, after which it is driven back when the electric force of the laser field changes direction. During the time in the continuum, the electron can acquire kinetic energy up to hundreds of eVs (the second step). Finally, the electron recombines with the parent ion with the emission of a photon (the third step). The electron recombines depending on the time it is released in the continuum. The field changes sign periodically, thus the emitted radiation will consist of the harmonics of the driving field according to the Fourier transform of the acceleration of the motion [30]. The maximum kinetic energy that an electron can gain before it recombines is $3.17U_p$. Adding to this energy $I_p$ that is gained during the recombination, the maximum energy can be written as:

$$E_{max} = I_p + 3.17U_p \tag{1.28}$$

From Eq. 1.28 and Eq. 1.27 it is apparent that there must be a cut-off region that is determined by the laser frequency and field strength. For example, for argon atoms $I_p = 15.78eV$, intensity $3 \times 10^{14} W/cm^2$ and central wavelength $\lambda_0 = 800nm$, the corresponding ponderomotive energy is $U_p \sim 18eV$. As a result, the maximum photon energy can reach $\sim 72eV$, which puts the radiation in the XUV range [7].

In Figure 1.5a we see a schematic illustration of a high harmonic spectrum [42]. The spectrum has a characteristic and universal shape: it falls off for the first few harmonics, then exhibits a plateau where all the harmonics have the same strength and ends up with a sharp cut-off.

Electrons generated at different phases around the peak of the field, gain different amounts of kinetic energy, but recombine with similar probability,

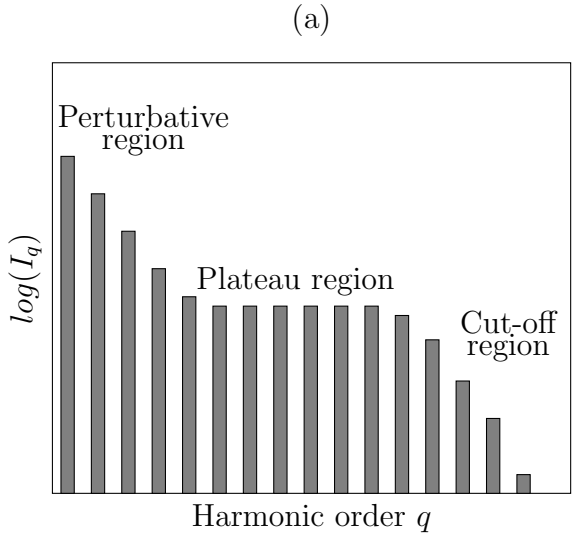


Figure 1.5: (a) Generic shape of the harmonic spectrum. It consists of the pertubative region, where the intensity drops according to the power law . The intensity remains constant over a range of harmonics in the plateau region. In the cut-off region it drops swiftly.

thus giving rise to constant conversion efficiency to photons over an extended spectral range. This explains the plateau region shown in Figure 1.5a.

Even though this semiclassical model provides a picture of the physics behind HHG and predicts the cutoff energy, it does not give information about the phase of the harmonic field and of the strength of the radiation. A quantum model developed by Lewenstein et al. [25] is at the moment the prominent theory used to describe the generation of the high harmonics. This model solves the time dependent Schrödinger equation for a single-active electron, high intensity limit ($U_p \geq I_p$) and for high harmonics with energies greater that the ionization potential.

# Chapter 2

# The Polarization Gating Technique

As mentioned earlier, it is of interest to produce a pulse with central wavelength at $270nm$ and a duration as short as possible. Using a driving laser with central wavelength of $800nm$ we can produce a pulse with the wavelength of interest by generating the third-harmonic of the fundamental. By widening the spectrum of the driving pulse, we produce wider band around the central wavelength, which can support a shorter third harmonic pulse. So, one solution to generate a short harmonic pulse is to use a few-cycle driving pulse (for $800nm$ a field oscillation takes $\simeq 2.7fs$). This is done with success, resulting in third-harmonic pulses with duration of sub $5fs$ [35, 19]. However in general, few-cycle lasers have a low energy content, namely less than $1mJ$, resulting in third-harmonic pulses with low energy content, as well. In many of the applications, we wish to have a more intense third-harmonic pulse, using the more energetic and commercially available many-cycle lasers. To give perspective, many-cycle laser have an energy content of few hundreds of $mJ$ per pulse ($\sim 10^{-2}J$). The scope of this thesis is to produce a third-harmonic pulse as short as possible using a many-cycle driving laser.

Using a driving pulse with FWHM $20fs$ (such as the laser in IESL), according to Eq. 1.16, we can achieve a pulse with duration of $11,5fs$. However, if we could somehow limit the generation of the third-harmonic in a short time interval, we could produce shorter pulses. One way to do this is to use the polarization gating technique which was mentioned earlier. The short temporal gate that the pulse is generated in, is based on the dependence of the efficiency of the generation on the ellipticity. The polarization gating technique has been extensively used in the field of HHG. There, using the polarization gating we prevent electrons, emitted after ionization, from

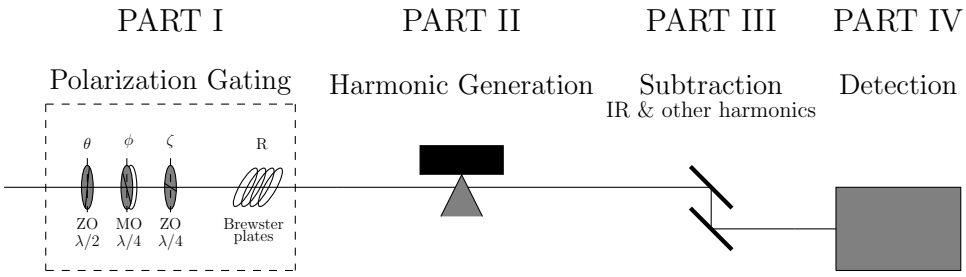


Figure 2.1: The arrangement used for the generation of the third-harmonic pulse. The first part consists of the polarization gating where the pulse acquires a time-dependent ellipticity suitable for the broadening of the generated spectrum. The second part is where the third-harmonic pulse is generated, consisting of an atomic gas jet. In the third part, pulses of different wavelength than the wavelength of interest are subtracted.

recombining with the parent ions for more than a few times during the driving pulse. Thus, a broadband continuum spectrum is generated, which may result in a single sub femtosecond pulse in the XUV wavelength range. Here, we attempt to use a similar idea in the perturbative regime, to generate short third-harmonic pulses.

## 2.1 Overview of the arrangement

In this thesis we make a simulation that is based on an experimental arrangement that is in development in IESL-FORTH. The arrangement consists of four parts. First is the polarization gating device which is used to create an ellipticity modulated driving pulse with linear polarization at the center of the pulse and elliptical elsewhere. Next, the pulse is focused in a gas jet where harmonics of the pulse are generated. Then the harmonics and the fundamental are co-propagating, thus we need to subtract the waves that we are not interested in. At the last part of the setup there is the detection of the harmonics and their temporal characterization. In the following section we will go in more details regarding the first part of the arrangement, the polarization gating device. The detection and the characterization will be discussed in the last chapter of this thesis.

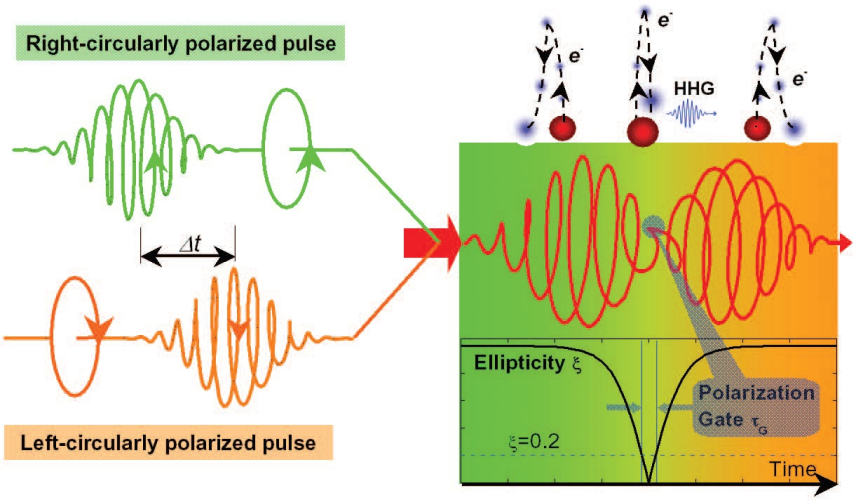


Figure 2.2: A pulse with a time-dependent ellipticity is formed by a left-circularly polarized pulse and a delayed right-circularly polarized pulse. Under this field, the re-collision process is only possible in the small region at the center where the ellipticity is close to zero [39].

## 2.2 Polarization Gating

The polarization gating (PG) is an optical arrangement that can modulate the ellipticity of a pulsed laser field to have linear polarization only at the center of the pulse. Taking advantage of the sensitivity of the harmonic generation to the ellipticity, the use of PG can provide a short time interval during which the harmonic emission takes place.

It was first proposed by Corkum in 1994 [12] for generating single isolated attosecond pulses. Initially, the proposal required two laser pulses with different center frequencies, but an alternative method using one center frequency, which is easier to implement, is mostly used now. The idea here is to implement a driver laser field with time dependent ellipticity by superposing a left and a right-circularly polarized pulse, which are delayed in respect to each other [39] (Figure 2.2a). In the composed pulse, the polarization varies from circular to linear and then back to circular. Thus, the necessary time interval for the generation is created in the center of the pulse.

### 2.2.1 Wave plate Polarization Gating Technique

The first realization of the polarization gating technique used two wave plates [29] (Figure 2.3). A linearly polarized input pulse is divided by the first wave plate, which is a multi-order $\lambda/4$ wave plate, in two pulses with perpendicular

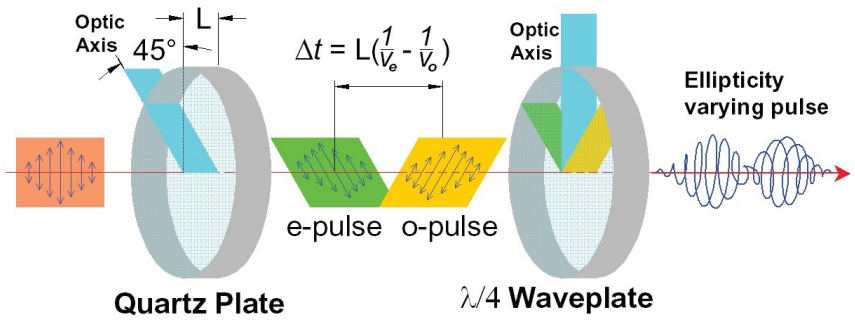


Figure 2.3: The arrangement of wave plates used to produce an ellipticity modulated pulse. [39]

linear polarization. The wave plate introduces a delay between the two pulses which is proportional to the thickness of the wave plate:

$$\delta = d\Big(\frac{1}{\nu_e} - \frac{1}{\nu_o}\Big) \ , \tag{2.1}$$

where d is the thickness of the plate, $\nu_e$ and $\nu_o$ are the velocities of the light in the extra-ordinary and ordinary axis of the plate respectively. The second wave plate is a zero-order $\lambda/4$ which converts the polarization from circular to linear in the central part of the pulse and linear to circular elsewhere. As a result, after the second wave plate, a pulse whose ellipticity changes with time is created.

However, this approach is not really applicable in many-cycle lasers. In order to produce a time interval short enough, down to few femtoseconds, a large delay between the two pulses introduced by the first wave plate is required. This translates into a thicker wave plate, which gives rise to two main problems. Firstly, when the delay has to be increased to high values, the overlap of the two pulses will occur only at the far edges that have low energy content and thus leads to a very low conversion efficiency. Secondly, another problem is that, due to the Kerr effect (dependence of the index of refraction on the intensity $n = n_1 + n_2 I$), the propagation of a pulse with high intensity through a medium, such as the wave plate, can result in damaging the wave-plate as well as distortion of the pulse through self phase modulation. A measure of how significant these nonlinear effects are, is the B-integral:

$$B = \frac{2\pi}{\lambda} \int n_2 I(z) dz \ , \tag{2.2}$$

where $I(z)$ is the optical intensity along the propagation axis, $z$ the position in the beam direction and $n_2$ is the nonlinear refractive index of the medium.

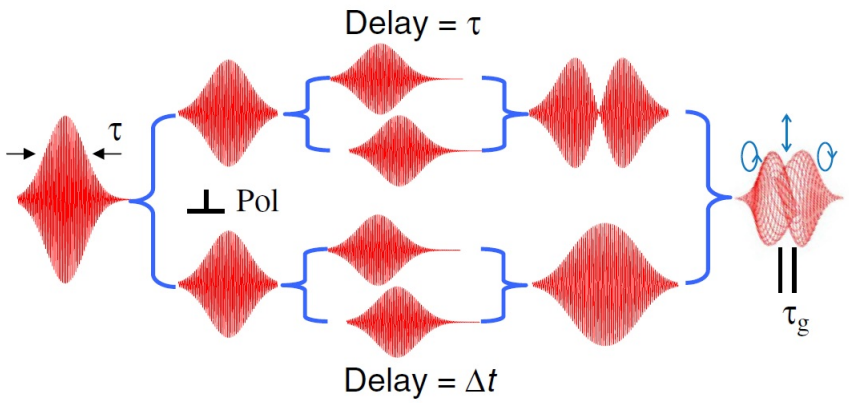


Figure 2.4: A schematic representation of the interferometric polarization gating approach. [10]

When $B > 1$ the Kerr effect is significant. Generally, when the length that the pulse propagates increases, the B-integral increases as well.

### 2.2.2 Interferometric Polarization Gating Technique

The first realization of the polarization gating to many-cycle lasers was the interferometric polarization gating technique. The method is shown in Figure 2.4. The initial pulse is split by amplitude into two pairs of pulses and the polarization of one pair is turned to perpendicular in respect to the polarization of the other. The pulses of one pair are delayed appropriately in order to interfere constructively, while the pulses of the second pair are delayed to form a destructive interference minimum. The two pulses are superimposed forming an ellipticity modulated pulse withlinear polarization in its central part. This is done by using either a Double Michelson Interferometer [43] or a double Mach-Zender [40] one. Here, we take advantage of the fact that the gate width depends not only on the delay between the two pairs, but also on the amplitude ratio between the delayed pulses. Even though this technique has been successful in generating intense single attosecond pulses, it suffers from energy losses and from experimental inconvenience due to difficult alignment.

### 2.2.3 CMC-PG

Here, we use another approach which is a modified wave plate polarization gating technique called collinear many-cycle polarization gating arrangement (CMC-PG). It is the wave plate approach, combined with the interfermetric

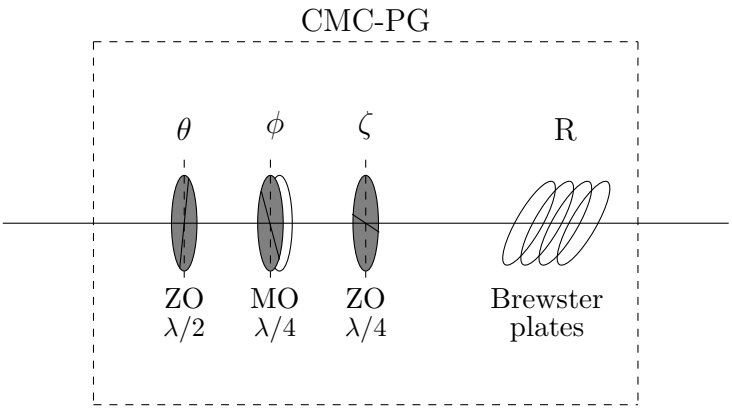


Figure 2.5: The collinear many-cycle polarization gating arrangement. ZO $\lambda/2$ is a zero-order half-wave plate. MO $\lambda/4$ is a multi-order quarter-wave plate that splits the pulse in two pulses that have perpendicular polarization and are delayed to each other. ZO $\lambda/4$ is a zero-order quarter-wave plate that converts the circular polarization near the center to linear. Here, the ratio of the fields is controlled by the Brewster plates.

polarization gating approach. Essentially, it provides the wave plate approach with the ability to control the ratio of the two fields. As a result, this approach is applicable when many-cycle lasers are used. The optical arrangement is shown in Figure 2.5. The CMC-PG setup has long term operational stability and set-up simplicity. It has been successfully used to generate a broadband continuum supporting isolated pulses [18].

### Amplitude Ratio

One way to implement the control of the ratio of the amplitudes relies in the Fresnel equations. When a beam approaches a surface, a part of it is reflected back and another is transmitted through (Figure 2.6a). The Fresnel equations relate the reflected $E_{0R}$ and transmitted $E_{0T}$ waves with the incident $E_{0I}$, which are different depending on whether the polarization of the wave is parallel or perpendicular to the plane of incidence. The Fresnel equations are [20]:

$$E_{0R} = \left(\frac{\alpha - \beta}{\alpha + \beta}\right) E_{0I} \ , \ E_{0T} = \left(\frac{2}{\alpha + \beta}\right) E_{0I} \ \text{ for parallel} \tag{2.3}$$

$$E_{0R} = \left(\frac{1 - \alpha\beta}{1 + \alpha\beta}\right) E_{0I} \ , \ E_{0T} = \left(\frac{2}{1 + \alpha\beta}\right) E_{0I} \ \text{for perpendicular.} \tag{2.4}$$

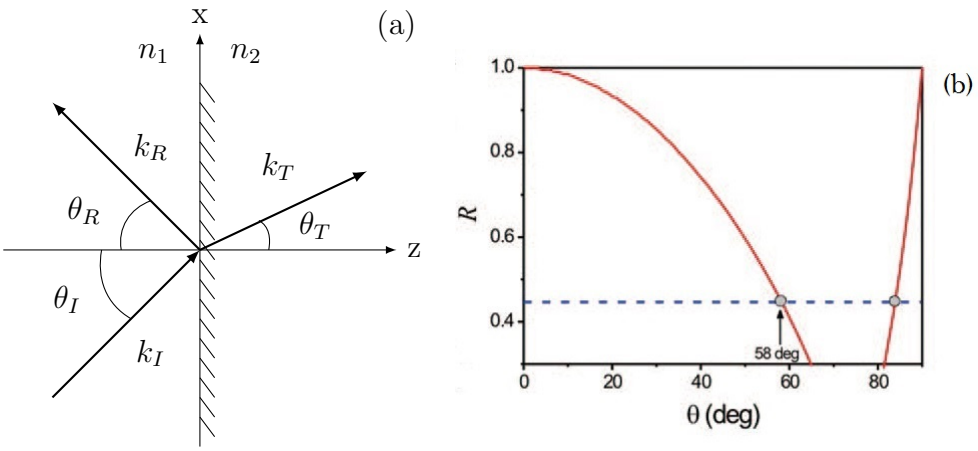


Figure 2.6: (a) Reflection and refraction of a wave. Depending on the polarization of the wave, the Fresnel equations determine the amplitudes of the reflected and transmitted waves. Here, the plane of incidence is the $xz$ plane. (b) Dependence of the ratio $R$ on the angle of incidence on a Si plate for the reflected part [18].

Using the above expressions we get the reflection and transmission coefficients which are:

$$R \equiv \frac{I_R}{I_I} = \Big(\frac{\alpha-\beta}{\alpha+\beta}\Big)^2 \ , \ T \equiv \frac{I_T}{I_I} = \alpha\beta\Big(\frac{2}{\alpha+\beta}\Big)^2 \ \text{ for parallel} \tag{2.5}$$

$$R = \Big(\frac{1-\alpha\beta}{1+\alpha\beta}\Big)^2 \ , \ T = \alpha\beta\Big(\frac{2}{1+\alpha\beta}\Big)^2 \ \text{for perpendicular,} \tag{2.6}$$

where $\alpha = \dfrac{\sqrt{1-[(n_1/n_2)\sin\theta_I]^2}}{\cos\theta_I}$ and $\beta = \dfrac{\mu_1 n_2}{\mu_2 n_1} \cong \dfrac{n_2}{n_1}$.
From the above equations, we see that by determining the angle of incidence of the pulse and the index of refraction, we can control the ratio of the amplitudes of the two components of the field. We can do this by either using the reflection, for example using a Silicon plate (Figure 2.6b), or the transmission which is done by using Brewster plates and a polarized beam splitter. By using the transmission, we can expect lower energy losses in the driving pulse.

## 2.3 Low-Order Harmonic Generation using Polarization Gating

In the previous section we discussed the idea, as well as different implementations of the polarization gating technique. The initial idea was introduced in the field of high-harmonic generation, as a way to generate single intense ultra-short pulses in the XUV wavelength range. The PG has been successful in doing so during the past decade.

However, this thesis is an attempt to utilize the polarization gating technique to generate a short low-order harmonic pulse. As mentioned before, the pulse duration of the generated low-order harmonic is $\tau_{q\omega} = \frac{\tau_\omega}{\sqrt{q}}$, where $q$ denotes the harmonic order and $\tau_\omega$ the generating pulse duration. By taking advantage the dependence of the harmonic generation on the laser pulse ellipticity, we create a short time interval for the harmonic generation to take place. In other words, we essentially limit the effective duration of the driving pulse to the width of the gate. As a result, we can expect that the polarization gating technique will work for low-harmonics as well.

Here, using the CMC-PG, we will investigate the production of a third-harmonic pulse by doing a simulation of the process, and we will also consider if any modifications are needed. This will be the subject of the next chapter.

# Chapter 3

# Calculations for the generation of third-harmonic pulses

To begin with, we suppose a laser with central wavelength at $\lambda_0 = 800nm$ and with duration $\tau_L = 20fs$. The laser is initially p-polarized. The electric field of the laser is then:

$$E(t) = \begin{pmatrix} E_p \\ 0 \end{pmatrix} = \begin{pmatrix} E_o e^{-i\omega_0 t} e^{-t^2/\tau^2} \\ 0 \end{pmatrix} , \tag{3.1}$$

where $\omega_0 = \frac{2\pi c}{\lambda_0}$ with $c$ being the speed of light in vacuum and $\tau = \frac{\tau_L}{\sqrt{2\ln 2}}$. This pulse will be propagated through the polarization gating. The ellipticity all along the pulse after the gating can be calculated by Eq. 1.19.

Equation 3.1 describes a pulse with a central frequency $\omega_0$ and a temporal envelope $e^{-t^2/\tau^2}$. Using Fourier analysis, it can be shown that such a pulse corresponds to a superposition of several monochromatic waves, the frequencies of which span according to: $\Delta\nu = \frac{0.441}{\tau}$, where $\Delta\nu$ is the spectral range. As a result, dispersion effects are expected to become important when transmission through dispersive media is considered. In CMC-PG, the implementation uses dispersive media, as a result we must include this in our calculation. As mentioned in the previous chapter, when a pulse is propagating through a dispersive medium, the electric field exiting can be described in the frequency domain as:

$$\tilde{E}_{out}(\omega) = \tilde{E}_{in}(\omega) e^{i\frac{\omega}{c}\tilde{n}(\omega)L} , \tag{3.2}$$

where $L$ is the length of the medium and $\tilde{n}(\omega)$ is the index of refraction of the material. From the above equation we see that we need the Fourier transform of the electric field in Equation 3.1, the refractive index and the thickness of the medium. Here, we suppose that the wave plates are made

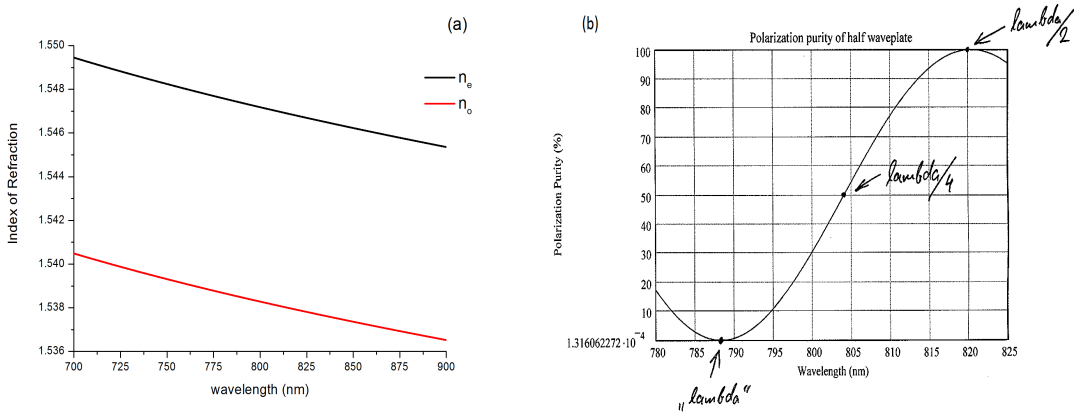


Figure 3.1: The index of refraction for the ordinary and extra-ordinary axis of crystal quartz.

from Crystal Quartz, as it was the case in Reference [18]. Then we can calculate the refractive index for both of the ordinary and extra-ordinary axes by the Laurent series equation:

$$n^2 = A_0 + A_1\lambda^2 + \frac{A_2}{\lambda^2} + \frac{A_3}{\lambda^3} + \frac{A_4}{\lambda^6} + \frac{A_5}{\lambda^8} \ , \tag{3.3}$$

where $\lambda$ is the wavelength expressed in $\mu m$ and $A_i$ are dispersion equation constants for Crystal Quartz (Figure 3.1a).

Next, we need the thickness of the wave plates. In general, a wave plate is created by combining two birefringent crystals with different lengths and the ordinary axis of one crystal being parallel with the extra-ordinary axis of the other. As a result, by determining the length of the two bifrengent crystals we can determine the phase difference between the two components. For one wavelength, when one component is advanced in comparison to the other by half the wavelength, the plate is a zero-order (ZO) $\lambda/2$ and when by a quarter of the wavelength it's called a zero-order (ZO) $\lambda/4$. When the delay is $n\lambda + \lambda/4$ or $n\lambda + \lambda/2$, where $n$ is the number of wavelengths that a component is delayed, the wave plate is called $\lambda/4$ or $\lambda/2$ multi-order (MO) respectively. However, multi-order wave plates are made by a single crystal. Consequently, a $\lambda/4$ MO wave plate introduces a delay of and a $\lambda/2$ MO wave plate introduces , . For the zero-order $\lambda/2$ plate, we assume a thickness of $0.62mm$ and for the zero-order $\lambda/4$ we assume a thickness of $0.67mm$, as was the case in Reference [18]. For the $\lambda/4$ multi-order, however the dispersion plays a more important role. Because of the large thickness of the plate, the wave plate does not give the same phase delay for all the spectral components. This can be seen in Figure b. The thickness is found

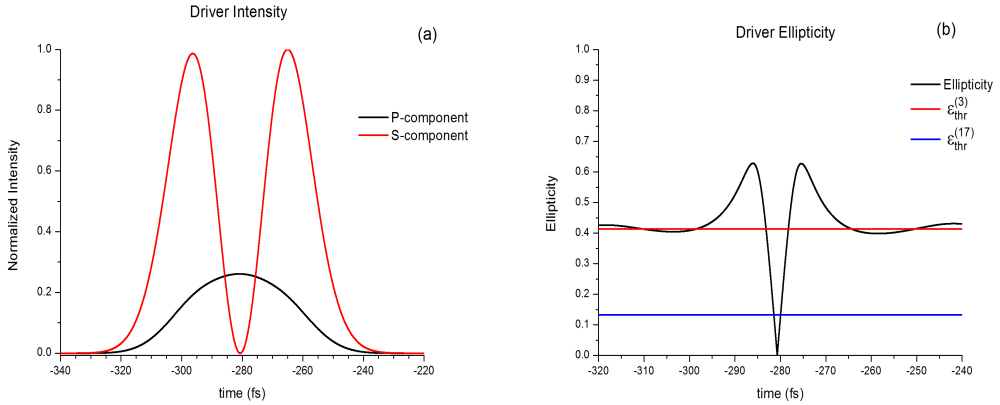


Figure 3.2: $\mathbf{I_p/I_s = 1/6}$ (a) The intensity of each component of the driving field after the gating. (b) The ellipticity of the field as a function of time (black line). The red line is the ellipticity threshold for the third-harmonic. The blue line is the ellipticity threshold for the 17th harmonic.

from Eq. 2.1 for a certain delay we choose between the two pulses. Here we choose a delay of 9 cycles, translating to a thickness of $0.83mm$.

Next, we move to the part where the harmonics are generated. In general by using a many-cycle pulse linearly polarized, the harmonics are generated, producing a spectrum like the one in Figure 1.5. As mentioned before, the efficiency of the HG depends on the ellipticity of the driving field. However, it is important to mention here that this efficiency dependence is not the same for all the harmonics. For low-harmonics the efficiency of the generation is described by:

$$I_{gen} = \left(\frac{1-\epsilon^2}{1+\epsilon^2}\right)^{(q-1)} I_{dr} \ , \tag{3.4}$$

where $I_{dr}$ is the intensity of the driver pulse.

## 3.1 Optimizing the intensity ratio for the generation of short third-harmonic pulses

Using the considerations mentioned above, we attempt to use the PG in order to produce short third-harmonic pulses. For this, we will set the angles of the wave plates (Figure 2.5): $\theta = \pi/8$ , $\phi = 0$ , $\zeta = \pi/4$. With this configuration, according to the simulation, the two components of the field are along the p and s polarization and the gate is expected to "open" along the p-direction. In other words, the pulse within the gate will be p-polarized.

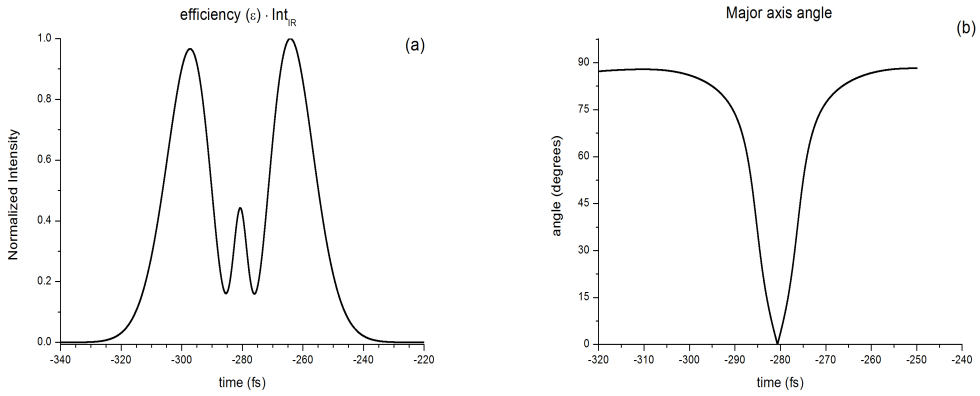


Figure 3.3: $\mathbf{I_p/I_s = 1/6}$ (a) Plot of the driver intensity $Int_{IR}$ multiplied by the efficiency of the generation $eff(\epsilon)$. (b) The angle of the major axis of the ellipse of the electric field in respect to the p-polarization as a function of time. At different times, different components dominate.

Using our simulation, we investigate the ratio that optimizes the harmonic outcome.

### $\mathbf{I_p/I_s = 1/6}$

A reasonable choice of ratio is $R = 1/6$. This is a common ratio when the gating apparatus is used to generate radiation in between the harmonics of high-order [43, 40], so it is interesting so investigate whether it works for the generation of low-harmonic pulses, as well.

In Figure 3.2a we see the intensity of the components of the field. In Figure 3.2b, we can see the ellipticity as a function of time. For the third-harmonic, according to Eq. 3.4, the gate width for this ratio is $\tau_g = 4.9fs$. As a result, one would expect that a pulse with such an ellipticity would produce a third-harmonic pulse with duration $\tau_{3rd} \approx \frac{\tau_g}{\sqrt{3}}$. Nevertheless, the Figure 3.3a shows a plot of the "generating intensity" $I = eff(\epsilon) \cdot I_{IR}$ as a function of time. It clearly indicates that there will be generation outside of the gate as well. This happens because, the efficiency of the generation does not drop rapidly enough with the ellipticity and in the case that driver intensities are sufficiently high outside the gate, considerable amount of harmonic generation can occur there as well. This is indeed the case for low-harmonic generation. As seen by Figure 1.2b, for the third harmonic, the ellipticity threshold is big enough to allow generation outside of the gate. This does not happen in high-order harmonic generation, above the $17nth$ harmonic, where $\epsilon_{thr} \approx 0.1$. This is a core difference that arises when considering har-

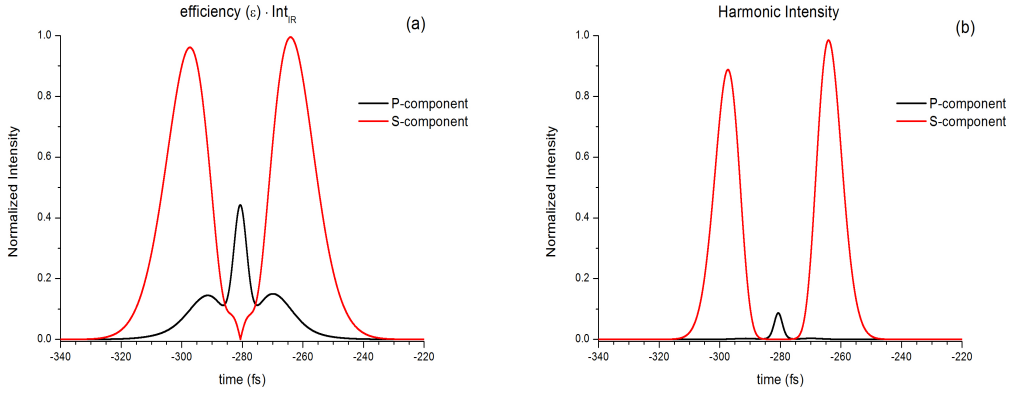


Figure 3.4: $\mathbf{I_p/I_s = 1/6}$ (a) Plot of the intensity of driver's components multiplied by the efficiency of the generation $eff(\epsilon)$. (b) The harmonic pulse, which has a p as well as a s-component.

monic generation of low in contrast to high harmonics and leads to a need of modification when considering the use of the gating technique.

However, we must take into consideration the fact that no matter if the harmonics are generated from a field with elliptical polarization, they will always be linearly polarized, according to the selection rules. The orientation of their polarization is that of the major axis of the ellipse. Using the Gating Technique with a ratio $I_p/I_s = 1/6$ the orientation of the ellipse changes with time. As a result, the orientation of the polarization of the harmonics will vary with time as well. In Figure 3.3b we see the angle $\phi_{el}$ as a function of time. According to the orientation of the ellipse, the component that generates the harmonic varies from s to p (in-gate) and back to s-polarization. Because of this, the harmonic outcome will have both a p and a s-component. Using the angle of the major axis we can calculate the "generating intensity of the components": $I_p = eff(\epsilon) \cdot I_{IR} \cdot \cos(\phi_{el})$ and $I_s = eff(\epsilon) \cdot I_{IR} \cdot \sin(\phi_{el})$. The result is shown in Figure 3.4a. Using the power law we find the expected harmonic outcome which is shown in Figure 3.4b. We see that in the p-polarization there is a single pulse with duration of $\tau_{3rd}^{p} = 3.2fs$. Nevertheless, this pulse is not the only one generated. In the s-polarization there are two other pulses, the first of which has a duration of $\tau_{3rd}^{(1)s} = 10.3fs$ and the second $\tau_{3rd}^{(2)s} = 9.6fs$. If, somehow, we could subtract the s-polarized pulses, we would have a very short third-harmonic p-polarized pulse, which however would have a much lower energy content. In applications where a high energy content is not needed, such a short pulse would be useful. On the other hand, if we subtract the pulse in the p-polarization we will obtain

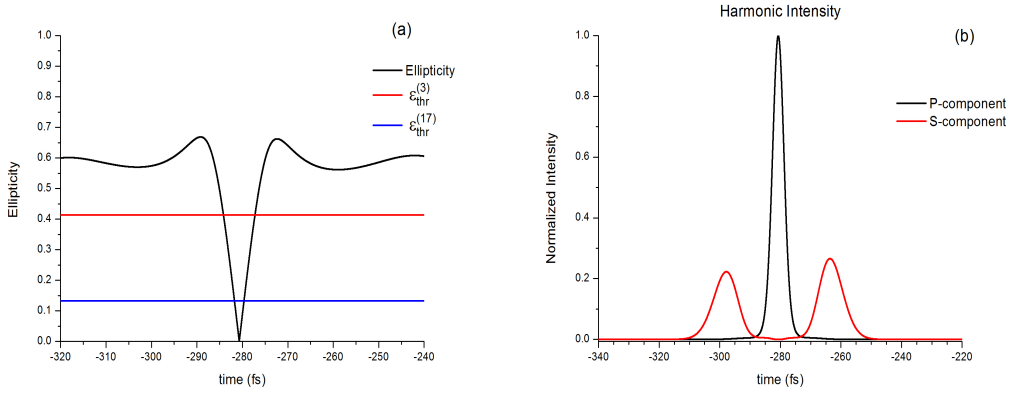


Figure 3.5: $\mathbf{I_p/I_s = 1/3}$ (a) The ellipticity of the field as a function of time (black line). The red line is the ellipticity threshold for the third-harmonic. The blue line is the ellipticity threshold for the 17th harmonic. (b) The harmonic outcome, there is still a p as well as a s-component, however the single pulse is more intense than the pulses of the s-polarization.

two pulses of duration $\approx 10fs$ that are delayed by $\approx 32fs$.

## $\mathbf{I_p/I_s = 1/3}$

In the previous section we saw that having a small ratio between the amplitudes of the components, we produce a short gate width. However, this does not translate to the generation of a short harmonic pulse only inside the gate. As a result, we suspect that by making the ratio bigger, we can limit the contribution of the harmonic outcome inside the gate. With this in mind, we set the ratio $R = 1/3$. Using the same approach as before we find the gate width for this ratio is $\tau_g = 6.9fs$. In Figure 3.5a we see the ellipticity of the driving pulse after the polarization gating. We can expect a smaller contribution in the harmonic outcome from outside of the gate. This is indeed the case, as shown in Figure 3.5b. We see that, as before, there are pulses in both p and s-polarization. The single pulse with p-polarization has a duration of $\tau_{3rd}^{p} = 4.5fs$. In the s-polarization, the first pulse has a duration of $\tau_{3rd}^{(1)s} = 10.3fs$ and the second $\tau_{3rd}^{(2)s} = 9.2fs$. Even though there is still harmonic outcome on the s-polarization, the intensity of these pulses are significantly smaller than the ratio $R = 1/6$. As we will see later, we can reduce further the intensity of the out-gate pulses and obtain a single intense pulse by using the fact that the polarization of the in-gate generated pulse is perpendicular to the polarization of the "twin" out-gate generated pulses.

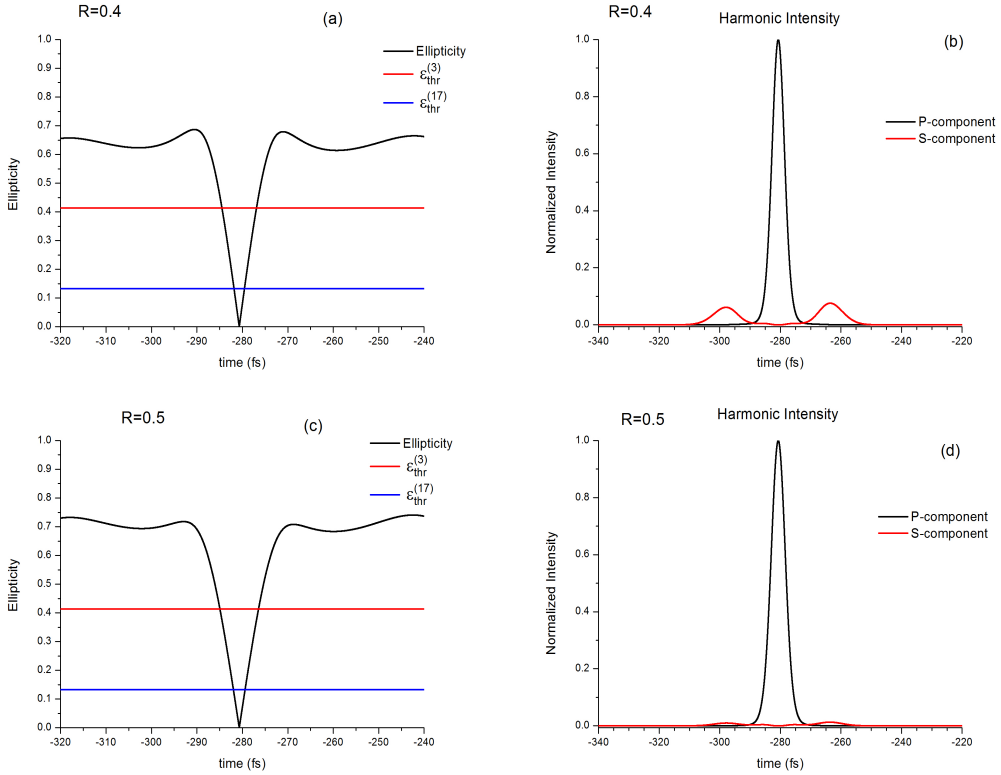


Figure 3.6: (a,c) The ellipticity of the field as a function of time (black line). The ellipticity is clearly bigger than the third-harmonic threshold outside of the gate, thus lowering the generation from outside the gate. (b,d) The harmonic outcome. The pulse in the p-polarization is significantly more intense than the harmonic outcome on the s-polarization.

## $\mathbf{I_p/I_s = 0.4,\ I_p/I_s = 0.5}$

Having the previous results in mind, we continue to lower the ratio. As we saw earlier, by doing so we make the gate wider, but we lower the contribution from outside of the gate to the harmonic outcome. As a result, we sacrifice on the p-polarized pulse duration in order to lower the harmonic outcome on the s-polarization. In Figure 3.6a there is the ellipticity of the pulse for R=0.4 and in 3.6c for R=0.5. In Figure 3.6b the harmonic outcome is plotted for R=0.4 and in 3.6d for R=0.5. The gate width is $\tau_g = 7.6fs$ for R=0.4 and $\tau_g = 8.5fs$ for R=0.5. As before, the p-polarized pulse is much more intense than the s-polarized pair of pulses. For R=0.4, the pulse which is p-polarized has a duration of $\tau_{3rd}^{p} = 4.9fs$, the first pulse on the s-polarization has a duration of $\tau_{3rd}^{(1)s} = 10.5fs$ and the second $\tau_{3rd}^{(2)s} = 9.2fs$. For R=0.5,

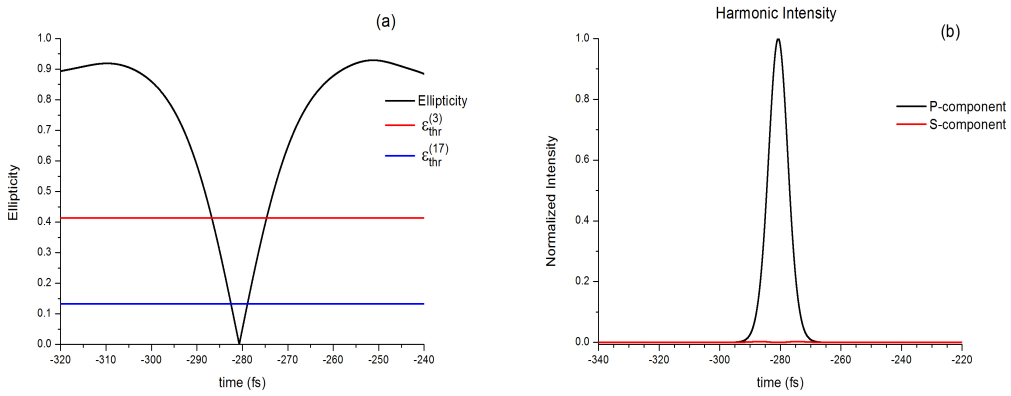


Figure 3.7: $\mathbf{I_p/I_s = 1}$ (a) The ellipticity of the field as a function of time (black line). The gate is wide enough in order to have no generation outside of it. (b) The harmonic outcome. Here, there is only harmonic outcome in the p-polarization.

the pulse in the p-polarization has a duration of $\tau_{3rd}^{(2)s} = 5.4fs$, while the harmonic outcome in the s-polarization is insignificant.

### $\mathbf{I_p/I_s = 1}$

For the sake of completeness we investigate the case where $R = 1$, ie. when do not modify the intensity ratio $I_p/I_s$. The ellipticity is shown in Figure 3.7a and the harmonic outcome in Figure 3.7b. In this case the gate width is $\tau_g = 11.7fs$ and there is a single pulse with duration of $\tau_{3rd}^{p} = 7.6fs$. We see that by not modifying the amplitude ratio, we have only generation inside the gate, leading to a single pulse. The pulse produced this way is still shorter than a third-harmonic pulse produced with no polarization gating ($11.7fs$ according to Eq. 1.16).

## 3.2 Synopsis

In the previous section we investigated whether CMC-PG works at the production on single, intense and short third-harmonic pulses by using various ratios of the amplitudes of the p and s-components of the driving field. In this section we attempt to evaluate if it has been successful and under what circumstances.

First of all, it is apparent that because of the differences between high and low-harmonic generation process, the CMC-PG needs modification. To be specific, by using the same intensity ratio $I_p/I_s$ as in high-harmonic gen-

eration, as was done in previous works [1], we do not obtain a single in-gate generated pulse. One remedy for this is to lower the ratio. By doing so, we can have a single pulse in the p-polarization, while lowering the intensity of the out-gate generated harmonic outcome. However, by lowering the ratio we sacrifice on the duration of the p-polarized single pulse. As result, this poses a limit on how short a third-harmonic pulse, which is produced using polarization gating, can be.

We can take advantage the fact that the single pulse is perpendicularly polarized with respect to the pair of pulses. Then, by taking advantage of the Fresnel equations we can choose to reduce the s-polarized components of the pulse. We will elaborate further on this in the following chapter.

# Chapter 4

# Experimental specifications

In this final chapter we will be discussing the experimental implementation of third-harmonic pulse generation, using the CMC-PG. As mentioned earlier, the simulation in this thesis is based on an experimental setup that is under development at IESL-FORTH. The first point to be addressed is how we will control the amplitude ratio. Next, comes the selection of the atomic gas to be used for the generation of the harmonics. Then, we will discuss the way to filter out the IR and harmonics of order higher than the third. Lastly, we will discuss the detection and the temporal characterization of the pulse. Of course, due to the high intensity of the laser pulse, the whole setup will be in vacuum with pressure at least $10^{-6}mbar$.

## 4.1 Amplitude ratio

As mentioned before, one way to control the amplitude ratio is by taking into account the Fresnel equations for reflection and transmission on the surface which separates two adjacent media with different refractive indices. Here, in order to control the ratio $R$ we use Brewster plates. The Brewster plates used are from NBK7, the index of refraction of which can be found from the Sellmeier equation (Figure 4.1a):

$$n^2 = 1 + \frac{B_1\lambda^2}{\lambda^2 - C_1} + \frac{B_2\lambda^2}{\lambda^2 - C_2} + \frac{B_3\lambda^2}{\lambda^2 - C_3} \ , \tag{4.1}$$

where $\lambda$ is the wavelength expressed in $\mu m$, $B_i$ and $C_i$ are the dispersion equation constants for NBK7.

We make use of the part of the pulse that is transmitted through the Brewster plates. Then the ratio of the p and s-polarized components is:

$$R = \frac{I_p}{I_s} = \frac{T_p}{T_s} \tag{4.2}$$

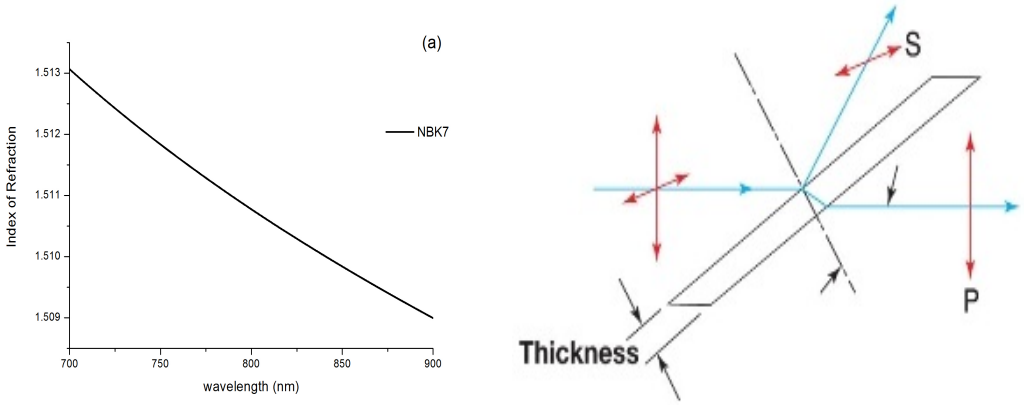


Figure 4.1: $\mathbf{R = 1}$ (a) The index of refraction for NBK7. (b) A schematic representation of a Brewster plate, shown the three axis which it can be rotated.

where $T_p$ and $T_s$ are the transmission coefficients for p and s-polarization respectively. Using the Fresnel equations we can find the ratio as a function of the angle of incidence. What is important here, is that, what we call parallel or perpendicular in the Fresnel equations is in respect to the plane of incidence.

In Figure 4.2a the ratio as a function of the angle of incidence is plotted. For a single plate, the ratio $R = 2$ can be achieved at the angle $71.6^o$. This translates to a length that the pulse will propagate of $634.2\mu m$.

For an intensity of the pulse $I_0 = 10^{12} W/cm^2$, the B-integral value is above 1. As a result, we need to use more plates. By doing so the total transmittance is $T_{tot} = T_1 T_2 \cdots T_n$, where $T_i$ is the transmittance for the i-th Brewster plate. We see that by using more plates, for the same ratio, the angle of incidence gets smaller. As a result, the beam propagates in less material, translating to a smaller B-integral as shown in Table 4.1.

| # plates | angle | B-integral |
|---|---|---|
| 1 | $71.6^o$ | 1.69 |
| 2 | $57.3^o$ | 0.98 |
| 3 | $49.3^o$ | 0.81 |
| 4 | $44.1^o$ | 0.74 |
| 5 | $40.1^o$ | 0.70 |
| 6 | $37.2^o$ | 0.67 |

$I_p/I_s = 2$

Table 4.1: A table with the value of B-integral for various number of plates in order to introduce a ratio of $I_p/I_s = 2$.

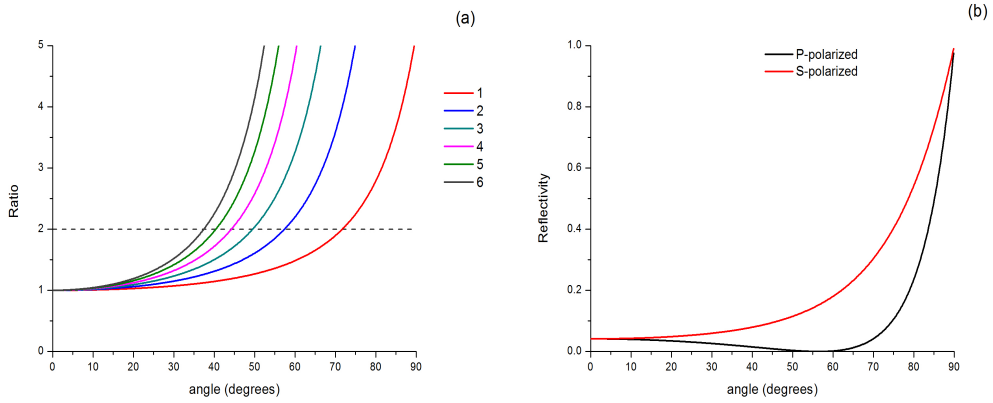


Figure 4.2: (a) The ratio as a function of the angle of incidence for different numbers of plates. The more plates we use, the smaller the angle of the plates, in order to have the same ratio. (b) The reflectivity of a NBK7 Brewster plate for $800nm$. Using this we can estimate the energy losses of the pulse due to reflections.

In the calculation of the B-integral it is apparent that there is a limit to the intensity of the beam that we can use. For intensities higher than $10^{12}W/cm^2$, the B-integral starts becoming larger.

However, when we use more plates, we sacrifice on the energy content. Due to the reflections on the two surfaces of each plate, a part of the pulse will be lost. In Figure 4.2b the reflectivity from a N-BK7 plate is plotted. For the angle $37.2^o$, which is the angle that $I_p/I_s = 2$ can be achieved by using 6 plates, in every reflection we can expect an energy loss of $\approx 2\%$ in the p-component and a loss of $\approx 7\%$ in the s-component. This translates to an energy loss of $\approx 11.8\%$ in the energy content in the p-component and $\approx 39.5\%$ in the s-component for all 6 plates.

## 4.2 Gas selection for the generation of the harmonics

After the polarization gating, the pulse becomes ellipticity modulated, with linear polarization at the center of the pulse. Next, the beam is focused in a gas jet where the harmonics of the fundamental will be generated. The selection of the gas plays a crucial role on the conversion efficiency of the fundamental into the third-harmonic pulse. As a result, it is crucial to use the gas that maximizes the energy output.

First of all, not all atomic media are suitable for the upconversion of

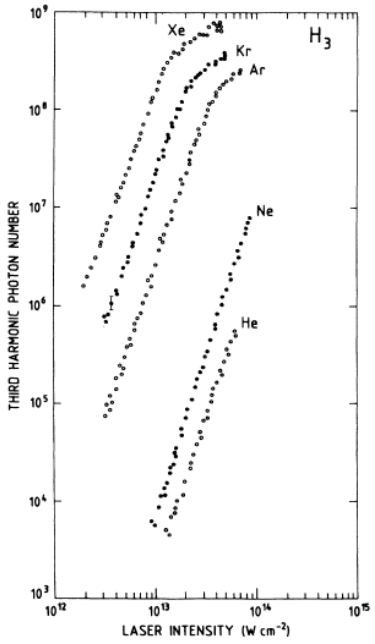


Figure 4.3: Laser-intensity dependence of the number of photons at the third harmonic in Xe, Kr, Ar, Ne, and He, at a 15 Torr pressure. Caption and figure from Reference [26].

a laser pulse with central wavelength of $\lambda_0 = 800nm$. Such a wavelength corresponds to a photon energy of $E_0 = \hbar\omega_0 = 1.55eV$. As a result, the most important qualification for an atomic medium in order to be suitable, is to have ionization energy $E_I > 3E_0$. When this condition does not hold, we cannot have third-harmonic generation, below threshold.

A parameter that need to be optimized is the the gas pressure. Generally, we can expect that by increasing the pressure we will have an increase in the upconversion efficiency, due to more more harmonics generated. However, beyond a critical pressure value, the ionization of the gas destroys phase-matching conditions significant, thus lowering the harmonic output (see *section 1.3*).

In Figure 4.3 the number of photons of the third-harmonic pulse is measured for various noble gasses versus the laser intensity [19]. The pressure used in this experiment was 15 Torr and the central wavelength of the laser was $1064nm$. According to this plot, the gas that has the highest conversion efficiency is xenon. In our experiment we will use gas pressure of one order of magnitude higher than 15 Torr, which was used in this experiment and laser intensities of between $10^{14} - 10^{15} W/cm^2$.

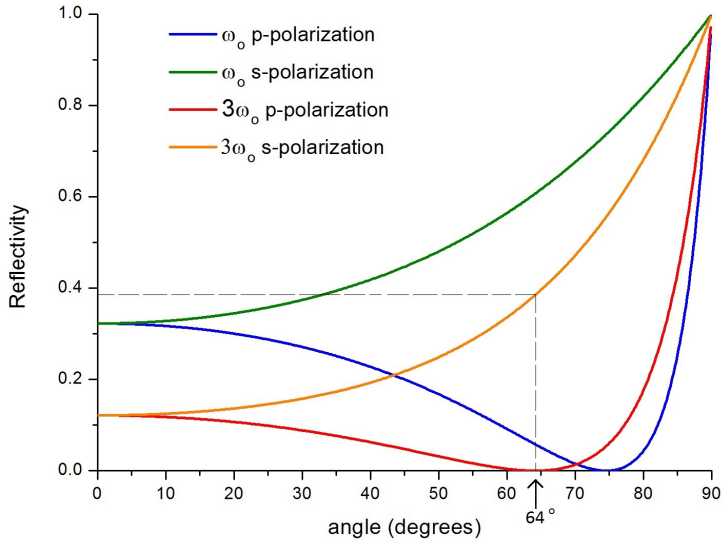


Figure 4.4: The reflectivity of a silicon plate versus the angle of incidence for the wavelength $\lambda_0 = 800nm$ and for $\lambda_3 = 266nm$. For $\lambda_0$ the Brewster angle is at $\approx 74.5^o$, while for $\lambda_3$ it is at $\approx 64^o$.

## 4.3 Selection of the single third-harmonic pulse

As mentioned before, when we focus a laser in a gas jet the harmonics are generated. After the harmonics are generated, they co-propagate with the fundamental. As a result, in order to have a pulse of the third-harmonic we have to separate it from the fundamental field and the other harmonics.

First, we use a silicon plate. This is a common procedure in order to subtract the fundamental in HHG experiments [41]. However, because after the polarization gating apparatus the driving field has p and s-components the silicon plate does not work well here. In Figure 4.4 the reflectivity of a silicon plate as a function of the angle of incidence is plotted. If we have the silicon plate is at the Brewster angle of the fundamental ($\approx 74.5^o$), the p-polarized component will be eliminated, while the s-component will be reduced by a factor of $\approx 27\%$. However, it is important to note that, due to the dependence of the refractive index on the wavelength, the Brewster angle is not the same for the third-harmonic pulse, which has central wavelength of $266nm$. The Brewster angle for this wavelength is $\approx 65^o$. If the silicon plate is at this angle, the p-polarized component of the harmonic outcome will be eliminated, while the s-polarized component will be reduced by $\approx 62\%$. Also, the p-polarized component of the fundamental will be reduced by $\approx 95\%$, while the s-component by $\approx 40\%$.

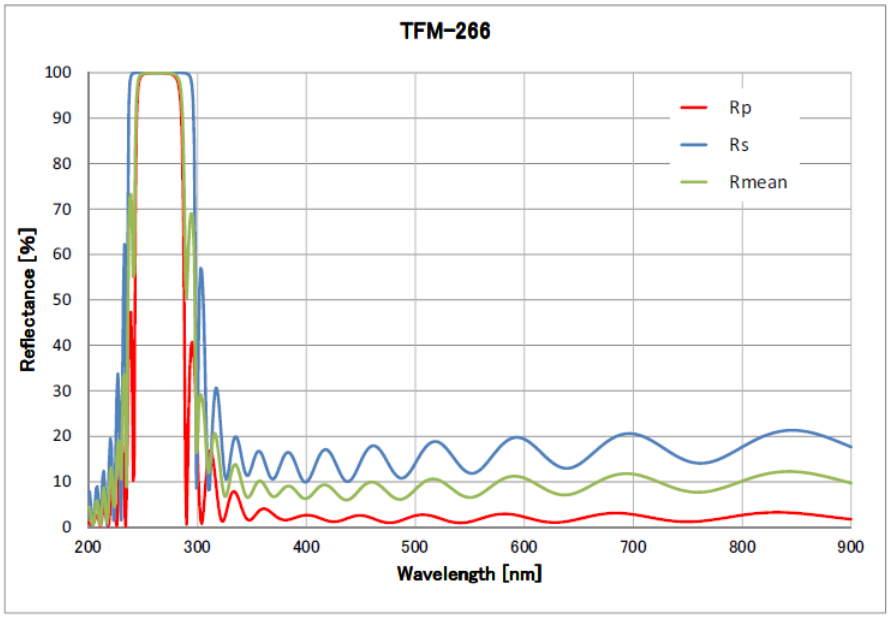


Figure 4.5: The reflectivity for the $3\omega$ mirror as a function of the wavelength. The mirrors are made from BK7 by OptoSigma. [28]

As we saw in *Chapter 3*, in the harmonic outcome there is a single pulse in one polarization and a pair of pulses in the perpendicular one. If we could have the "twin pulses" in the polarization that the silicon will suppress, then we will essentially have only the single pulse left. This can be done by either having the plane of incidence perpendicular to the p-polarization or by generating them in the p-polarization in the first place. It is much easier to generate the single pulse in the s-polarization and the pair in the p-polarization. We can do this by making sure the pulse will be s-polarized within the gate. In order to achieve this we need a proper configuration of the angles of the wave plates, for example: $\theta = \pi/8$, $\phi = \pi/2$ and $\zeta = \pi/4$ where $\theta$ is the angle is the $\lambda/2$ ZO, $\phi$ is the angle of the $\lambda/4$ MO and $\zeta$ the angle of the $\lambda/4$ ZO wave plate.

In order to filter out the IR and the higher-order harmonics, we use two mirrors that reflect mainly at the spectral area which supports a short-in-time duration third harmonic pulse. The Figure 4.5 shows the reflectance of a single mirror as a function of the wavelength. We see that at wavelengths around $260nm$ the reflectivity is close to 100%, while for wavelengths around $800nm$ the reflectivity is close to 20% for the s-polarization and $\approx 5\%$ for

p-polarization. By using two mirrors, the reflectivity for the s-component drops to 4% and for p-component less than 0.2%.

Concluding, by using the combination of the silicon plate and the pair of $3\omega$ mirrors, we can reduce the s-component of the fundamental down to $\approx 2.4\%$ of the initial intensity and the p-component to $< 0.1\%$. The losses for the third-harmonic pulse are $\approx 100\%$ for the p-polarized and $\approx 62\%$ for the s-polarization. Importantly, the silicon plate gives us the ability to suppress the p-component of the third-harmonic pulse more than 100 times more than the s-component. This provides a way to subtract the "twin pulses" that are generated with perpendicular polarization with the single pulse, leaving only a single short third-harmonic pulse after this stage.

## 4.4 Detection and temporal characterization

After the IR and the higher-order harmonics are filtered out, the single third-harmonic pulse goes in the detection chamber in order to be temporally characterized. However, we cannot, yet, be sure whether we have a pulse. In order to have a pulse, the relative phases of the different frequencies must be suitable. As a result, this part of the arrangement is crucial to determine whether we have a pulse and acquire its temporal characterization.

For the temporal characterization an auto-correlation technique will be used. By using a first-order auto-correlation measurement, we only have information about the coherence time [36]. In order to obtain the duration of the pulse, we must use a second-order auto-correlation measurement. To do this we must have a second-order nonlinear process. For this we can maybe use the two-photon ionization process of toluene, as it was used before [1].

However, if the energy content of the third-harmonic pulse is sufficient a third-order auto-correlation measurement can be used as well. In contrast to the second-order, where we only have information about the duration of the pulse, in the third-order we have information about asymmetries in the temporal profile of the pulse, in addition to the duration. As a result, the third-order auto-correlation provides a more complete temporal characterization of the pulse, but it requires a third-order nonlinear process, requiring more energetic pulses. As a third-order nonlinear process, a candidate is the three-photon ionization of xenon. The ionization energy of xenon is $12.1eV$, while the photon energy corresponding to a wavelength of $270nm$ is $4.6eV$. As a result, xenon can be ionized using three photons. However, it needs to be evaluated if the intermediate resonances do not affect its nonlinear properties when broadband pulses are used to ionize the xenon atoms.

## Estimation of energy content of the single third-harmonic pulse

Here we will attempt to give a quantitative estimation for the energy content of the third-harmonic pulse before going into the detection chamber. For the energy content of the driving laser we will assume an energy of $400mJ$, which is the maximum energy per pulse achievable for the laser system in IESL-FORTH. We can expect to lose close to 27% of the energy due to reflections on the wave plates leaving $\approx 291mJ$. In order to give an intensity ratio of $I_p/I_s = 1/3$ with 6 Brewster plates we need an angle of $45^o$. For such an arrangement of Brewster plates we can expect losses of $\approx 1\%$ in the p-polarization and $\approx 9\%$ in the s-polarization. This translates to an energy after the plates of $\approx 276mJ$. For the third-harmonic generation, we will assume a conversion efficiency of 10%. As a result, the third harmonic outcome will have an energy of $\approx 27mJ$. For the intensity ratio $I_p/I_s = 1/3$ the in-gate generated component is $\approx 3.8$ times more intense than the out-gate generated component. As discussed earlier, after the silicon plate, the out-gate generated component will be filtered out, leaving a single third-harmonic pulse with energy content of $\approx 18mJ$. The $3\omega$ mirrors have reflectivity almost 100% for the third-harmonic. As a result, we can expect that the third-harmonic pulse will have an energy content of at least $18mJ$ and a duration of $4.5fs$.

The experimental arrangement can be seen in Figure 4.6 . It is similar to the experimental arrangement used in Reference [1], with a few modifications.

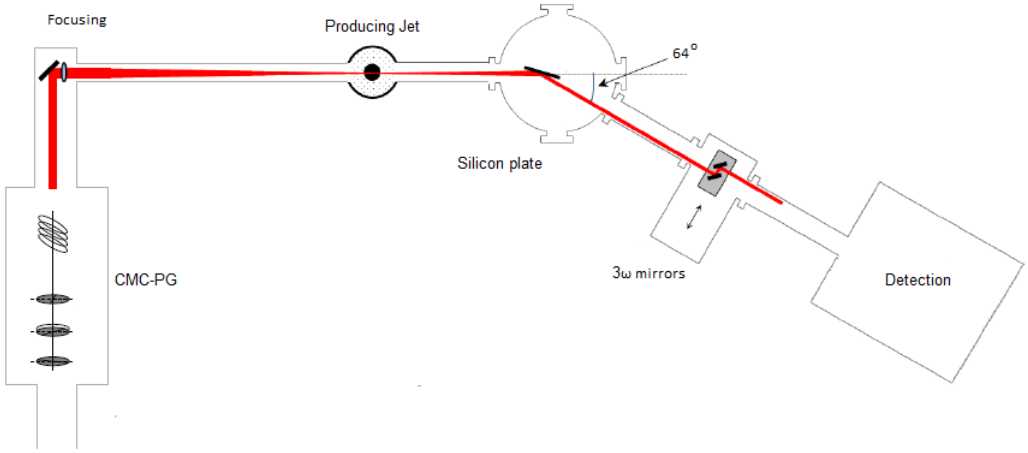


Figure 4.6: The experimental arrangement proposed. It consists of the polarization gating setup, the focusing of the beam, a gas jet where the generation takes place. Then there are the silicon plate and the $3\omega$ mirrors and lastly the detection chamber where the temporal characterization takes place.

# Bibliography


[1] Mavris A. Production and characterization of low order harmonics generated by using the polarization-gating technique. diploma thesis, University of Crete, Department of Physics, 2014.

[2] P Antoine, A. L'Huillier, M. Lewenstein, P. Salières, and B. Carré. Theory of high-order harmonic generation by an elliptically polarized laser field. *Phys. Rev. A*, 53:1725–1745, Mar 1996.

[3] Robert W. Boyd. The Nonlinear Optical Susceptibility. In *Nonlinear Optics (Third Edition)*, pages 1 – 67. Academic Press, Burlington, third edition, 2008.

[4] T. Brabec and F. Krausz. Intense few-cycle laser fields: Frontiers of Nonlinear Optics. *Rev. Mod. Phys.*, 72:545–591, Apr 2000.

[5] K. S. Budil, P. Salières, Anne L'Huillier, T. Ditmire, and M. D. Perry. Influence of ellipticity on harmonic generation. *Phys. Rev. A*, 48:R3437–R3440, Nov 1993.

[6] Z. Chang. Quest for Attosecond Optical Pulses. In *Fundamentals Of Attosecond Optics*, pages 1–46. CRC Press, 2011.

[7] Z. Chang. Semiclassical Model. In *Fundamentals Of Attosecond Optics*, pages 165–222. CRC Press, 2011.

[8] Z. Chang. Strong Field Approximation. In *Fundamentals Of Attosecond Optics*, pages 223–280. CRC Press, 2011.

[9] Z. Chang. Strong Phase Matching. In *Fundamentals Of Attosecond Optics*, pages 281–336. CRC Press, 2011.

[10] D Charalambidis, P Tzallas, E P Benis, E Skantzakis, G Maravelias, L A A Nikolopoulos, A Peralta Conde, and G D Tsakiris. Exploring intense attosecond pulses. *New Journal of Physics*, 10(2):025018, 2008.

[11] P. B. Corkum. Plasma perspective on strong field multiphoton ionization. *Phys. Rev. Lett.*, 71:1994–1997, Sep 1993.

[12] P. B. Corkum, N. H. Burnett, and M. Y. Ivanov. Subfemtosecond pulses. *Opt. Lett.*, 19(22):1870–1872, Nov 1994.

[13] Skantzakis E. *Generation and applications of intense isolated attosecond pulses*. PhD thesis, University of Crete, 2011.

[14] T. Popmintchev et al. The attosecond nonlinear optics of bright coherent x-ray generation. *Nature Photonics*, 4:822–832, Nov 2010.

[15] L. Pedrotti F. Pedrotti. Matrix Treatment of Polarization. In *Introduction to Optics*, pages 280–297. Prentice-Hall International, Inc, second edition, 1992.

[16] P. A. Franken, A. E. Hill, C. W. Peters, and G. Weinreich. Generation of Optical Harmonics. *Phys. Rev. Lett.*, 7:118–119, Aug 1961.

[17] Kolliopoulos G. *Visualization and Control of the Electron Quantum Paths in High Field Laser-Atom Interactions*. PhD thesis, University of Crete, 2014.

[18] Kolliopoulos G., Carpeggiani P. A., D. Rompotis, Charalambidis D., and Tzallas P. A compact collinear polarization gating scheme for many cycle laser pulses. *Review of Scientific Instruments*, 83(6):–, 2012.

[19] U. Graf, M. Fieß, M. Schultze, R. Kienberger, F. Krausz, and E. Goulielmakis. Intense few-cycle light pulses in the deep ultraviolet. *Opt. Express*, 16(23):18956–18963, Nov 2008.

[20] D. J. Griffiths. Electromagnetic Waves. In *Introduction to Electrodynamics*, pages 364–415. Prentice Hall, third edition, 1999.

[21] Misha Yu Ivanov, Michael Spanner, and Olga Smirnova. Anatomy of strong field ionization. *Journal of Modern Optics*, 52(2-3):165–184, 2005.

[22] J. D. Jackson. Plane Electromagnetic Waves and Wave Propagation. In *Classical electrodynamics*, pages 295–351. Wiley, third edition, 1999.

[23] L.V. Keldysh. Ionization in the field of a strong electromagnetic wave. *Soviet Physics JETP*, 20:1307–1314, May 1965.

[24] K.C. Kulander, K.J. Schafer, and J.L. Krause. Dynamics of short-pulse excitation, ionization and harmonic conversion. In B. Piraux, A. L'Huillier, and K. Rzazewski, editors, *Super-Intense Laser-Atom Physics*, volume 316 of *NATO ASI Series*, pages 95–110. Springer US, 1993.

[25] M. Lewenstein, Ph. Balcou, M. Yu. Ivanov, A. L'Huillier, and P. B. Corkum. Theory of high-harmonic generation by low-frequency laser fields. *Phys. Rev. A*, 49:2117–2132, Mar 1994.

[26] X. F. Li, A. L'Huillier, M. Ferray, L. A. Lompré, and G. Mainfray. Multiple-harmonic generation in rare gases at high laser intensity. *Phys. Rev. A*, 39:5751–5761, Jun 1989.

[27] Swinburne University of Technology. `http://www.swinburne.edu.au/engineering/caous/HHG.htm`.

[28] OptoSigma. `http://www.global-optosigma.com/en/page_pdf/TFM.pdf`.

[29] V. T. Platonenko and V. V. Strelkov. Single attosecond soft-x-ray pulse generated with a limited laser beam. *J. Opt. Soc. Am. B*, 16(3):435–440, Mar 1999.

[30] M Protopapas, C H Keitel, and P L Knight. Atomic physics with super-high intensity lasers. *Reports on Progress in Physics*, 60(4):389, 1997.

[31] J. F. Reintjes. Higher-order Processes. In *Nonlinear Optical Parametric Processes in Liquids and Gases*, pages 149 – 215. Academic Press, 1984.

[32] J. F. Reintjes. Introduction. In *Nonlinear Optical Parametric Processes in Liquids and Gases*, pages 1 – 29. Academic Press, 1984.

[33] J. F. Reintjes. Limitations on Convertion Efficiency due to Competing Effects. In *Nonlinear Optical Parametric Processes in Liquids and Gases*, pages 217 – 326. Academic Press, 1984.

[34] J. F. Reintjes. Third-harmonic Generation and Third-order Frequency Mixing. In *Nonlinear Optical Parametric Processes in Liquids and Gases*, pages 31 – 147. Academic Press, 1984.

[35] Florentin Reiter, Ulrich Graf, Martin Schultze, Wolfgang Schweinberger, Hartmut Schröder, Nicholas Karpowicz, Abdallah Mohammed

Azzeer, Reinhard Kienberger, Ferenc Krausz, and Eleftherios Goulielmakis. Generation of sub-3 fs pulses in the deep ultraviolet. *Opt. Lett.*, 35(13):2248–2250, Jul 2010.

[36] B. Saleh and M. Teich. Statistical Optics. In *Fundamentals of Photonics*, pages 343–381. Wiley, 2007.

[37] G. Sansone. Quantum path analysis of isolated attosecond pulse generation by polarization gating. *Phys. Rev. A*, 79:053410, May 2009.

[38] Kenneth J. Schafer and Kenneth C. Kulander. High harmonic generation from ultrafast pump lasers. *Phys. Rev. Lett.*, 78:638–641, Jan 1997.

[39] Bing Shan, Shambhu Ghimire, and Zenghu Chang. Generation of the attosecond extreme ultraviolet supercontinuum by a polarization gating. *Journal of Modern Optics*, 52(2-3):277–283, 2005.

[40] E. Skantzakis, P. Tzallas, J. Kruse, C. Kalpouzos, and D. Charalambidis. Coherent continuum extreme ultraviolet radiation in the sub-100-nj range generated by a high-power many-cycle laser field. *Opt. Lett.*, 34(11):1732–1734, Jun 2009.

[41] Eiji J. Takahashi, Hirokazu Hasegawa, Yasuo Nabekawa, and Katsumi Midorikawa. High-throughput, high-damage-threshold broadband beam splitter for high-order harmonics in the extreme-ultraviolet region. *Opt. Lett.*, 29(5):507–509, Mar 2004.

[42] U. Teubner and P. Gibbon. High-order harmonics from laser-irradiated plasma surfaces. *Rev. Mod. Phys.*, 81:445–479, Apr 2009.

[43] P. Tzallas, E. Skantzakis, C. Kalpouzos, E. P. Benis, G. D. Tsakiris, and D. Charalambidis. Generation of intense continuum extreme-ultraviolet radiation by many-cycle laser fields. *Nature Physics*, 3:846–850, Oct 2007.

[44] G. K. Woodgate. Radiative Transitions. In *Elementary Atomic Structure*, pages 32–56. Oxford University Press, second edition, 1989.

[45] J. Zhou, J. Peatross, M. M. Murnane, H. C. Kapteyn, and I. P. Christov. Enhanced high-harmonic generation using 25 fs laser pulses. *Phys. Rev. Lett.*, 76:752–755, Jan 1996.